Occupant response during autonomous braking manoeuvres in novel seating positions

Gregor Gstrein*, Christoph Leo*, Nico Erlinger, Desiree Kofler, Alois Jauernig, Corina Klug

Abstract To analyse the occupant response during braking manoeuvres and to derive realistic postures at the start of a potential subsequent collision, a series of 20 volunteer tests (10 female, 10 male) was carried out. The participants were subjected to two braking-pulses in an upright and a zero-gravity seating position. Kinematics was tracked, the muscle activation was measured at the most relevant muscle groups, and reaction forces on belt and feet support were recorded.

A considerable influence of the braking pulse on the occupant response was observed. While the medium braking pulse induced hardly any torso rotation and only minor neck flexion, the selected full braking pulse showed clear upper-body excursion, with small differences between male and female volunteers. Occupants in the zero-gravity seating position showed a slide-down motion of the torso relative to the seatback rather than rotation, resulting in a slightly earlier neck flexion.

With the body height axis oriented more parallel to the braking direction (zero-gravity posture), the upper torso rotation was reduced and neck loading increased as compared to a conventional upright seating posture. The severity of the autonomous emergency braking (AEB) pulse was found to be a major influence on the peak forward excursion of the occupants.

Keywords Active human body models, autonomous emergency braking (AEB), future seat setting, pre-crash occupant motion, volunteer testing.

I. INTRODUCTION

The advancement of autonomous vehicles promises occupants greater flexibility in choosing their seating postures, but this presents novel challenges for vehicle safety. Notably, reclined postures may become prevalent in future vehicles, but these seat configurations are suspected to influence kinematics and spine loads in case of an accident compared to conventional upright postures [1–3].

Pre-crash manoeuvres, such as braking or evasive steering, may affect the initial occupant posture considerably, which is critical for the effective deployment and performance of restraint systems in a subsequent crash [4]. Such evasive manoeuvres precede over half of passenger car accidents, with braking being the most frequent response [5–7].

Furthermore, studies have shown notable disparities in occupant excursions between human volunteers and crash test dummies during simulated pre-crash scenarios, including frontal acceleration tests [8–9], lateral sled tests [10–11], and lane change manoeuvres [12]. However, existing volunteer studies on pre-crash braking mainly focused on conventional upright seating postures, conducted both in laboratory environments and within driving cars. Several tests in laboratory environment have investigated upright driver postures [9], [13–16], passenger postures with hands resting on thighs [17–20], passenger postures with hands hanging to the sides [21], and upright driver postures with hands on the steering wheel and passenger postures [7]. In-vehicle studies on upright positions focused on relaxed initial muscle states and full braking events in conventional upright passenger postures [8], [22–32] have been published before.

Only a limited number of studies in reclined positions are available so far. Studies [23] and [33] examined out-of-position occupants and reclined seating during braking manoeuvres, highlighting considerable influence on peak forward head excursion based on initial occupant posture. Another study, [34], showed higher peak forward head excursions in full-reclined compared to half-reclined configurations during in-vehicle tests. Similarly, the in-vehicle tests conducted by [35] and [36] found a correlation between increased reclined angle and increased peak forward head excursion. In addition, [37], using a test buck based on a production vehicle (including the passenger seat), also determined that the peak forward head excursion was greater in reclined seating positions than in upright positions during the simulated AEB pulse braking manoeuvres. However, [38] observed a significant

*) G. Gstrein (e-mail: gregor.gstrein@tugraz.at; tel: +43 316 873-30314) and C. Leo are Senior Scientists and shared first authors, N. Erlinger, D. Kofler and A. Jauernig are Research Assistants, and C. Klug is Associate Professor, all at the Vehicle Safety Institute of Graz University of Technology, Austria.

decrease in peak forward head excursion in three of the four reclined postures compared to the upright posture. This sled study, involving three male volunteers, used a generic seat where the reclined positions were achieved by adjusting both the seat pan and seatback angles.

Active Human Body Models (HBMs) have been developed to investigate pre-crash-related responses (e.g. autonomous braking) and long-duration accident types (e.g. far-side impacts). Utilized models utilized both multi-body simulation [39–42] and finite-element simulation [4], [43–51]. However, the calibration of these active HBMs was predominantly focused on typical upright seat positions. For calibrating and validating the muscle models, laboratory volunteer tests are advantageous, as these controlled environments offer greater measurement possibilities and defined boundary conditions compared to in-vehicle testing.

This study aimed to investigate the kinematic and muscle responses of volunteers subjected to an acceleration pulse, simulating an AEB manoeuvre, and specifically focusing on differences between reclined and conventional upright seating postures and differences between male and female participants. Thereby the kinematics of different body regions (head, upper torso, pelvis) during the braking and the respective peak excursion was the main scope of research.

Ultimately, this research seeks to contribute to the calibration and validation of active HBMs, in particular for future seating postures, by providing a publicly available dataset that includes trajectory data, muscle responses times and activation levels as well as reaction forces of the volunteers with the sled.

II. METHODS

A. LowG Testbed

The volunteer study utilised an in-house-developed testbed called LowG (Fig. 1), which was specifically designed to simulate acceleration loadings on volunteers in a safe and controlled environment. The LowG enables an analysis of pre-crash kinematics and muscle activation in the pre-crash phase for both conventional and novel seating postures under varied load directions. The LowG can generate acceleration pulses of up to 1 g and a maximum velocity of 4.3 m/s over a travel distance of 3.8 m. Applied safety protocols, redundant control and monitoring units, ensure a high level of participant safety. The testbed features a customisable generic seat allowing for postural variations from upright to reclined to flat-lying. Independent adjustments of the inclination of the backrest and seat pan, along with an adjustable position and angle of the footrest, provide extensive flexibility. For highly reclined and flat-lying configurations, a lower leg support can be added, in order to provide an ergonomic and realistic seating position. Finally, the entire seat and footrest assembly may be rotated on the sled, enabling tests in multi-directional loading scenarios.

Fig. 1. LowG testbed in upright seating configuration.

B. Test conditions

The braking characteristics were based on [52], which derived clusters of pre-crash pulses from over 2,000 cars tested by IIHS between 2013 and 2019. Cluster 3, representing a "low severity" braking pulse, was used from this study. In addition, a generic pulse with an onset of 3 g/s, representing more recent AEB characteristics derived from braking pulses shown in [36], was included. Both pulses were trimmed to meet the constraints of the LowG testbed. The tested pulses and the very good repeatability are shown in Fig. 2a.

As reference, an upright seat position was based on [53] and [38], with a seat pan angle of 15.5° to the horizontal and a seatback angle of 20° to the vertical. For the future seat position, a Zero-G (0g) position based on [54] was utilised with a seat pan angle of 40° to the horizontal and a seatback angle of 65° to the vertical using an additional leg support. In Fig. 2b and c the two analysed seat settings are shown.

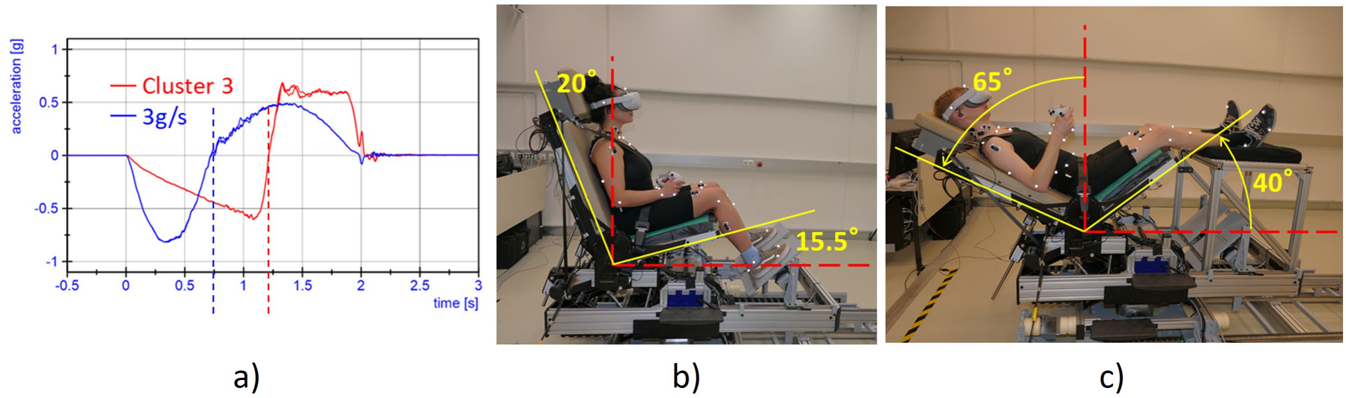

Fig. 2. Test-Boundary Conditions: a) investigated AEB pulses, whereby after the vertical dashed line the sled is braked. The curves of the three test repetitions overlap very closely, confirming a very good repeatability of the loading; b) upright seat position; c) zero-G seat position.

In order to distract the volunteers from the ongoing test and thereby achieve the most realistic behaviour possible (relaxed and unaware), they played simple games on a VR headset (META Oculus Quest 2) and listened to music, as described in [20]. An influence of the weight of the equipment (0.5 kg) was analysed in a separate test series and was found to be negligible.

C. Volunteers

Twenty volunteers with varying anthropometries participated in the study, with an equal number of males and females. The age range was 23–33 years for males (mean 26.5 years) and 20–42 years for females (mean 27.5 years). Further anthropometric data of the volunteers, including weight, height and BMI, can be seen in Fig. 3 and all captured data are included in the Appendix, in Table AI.

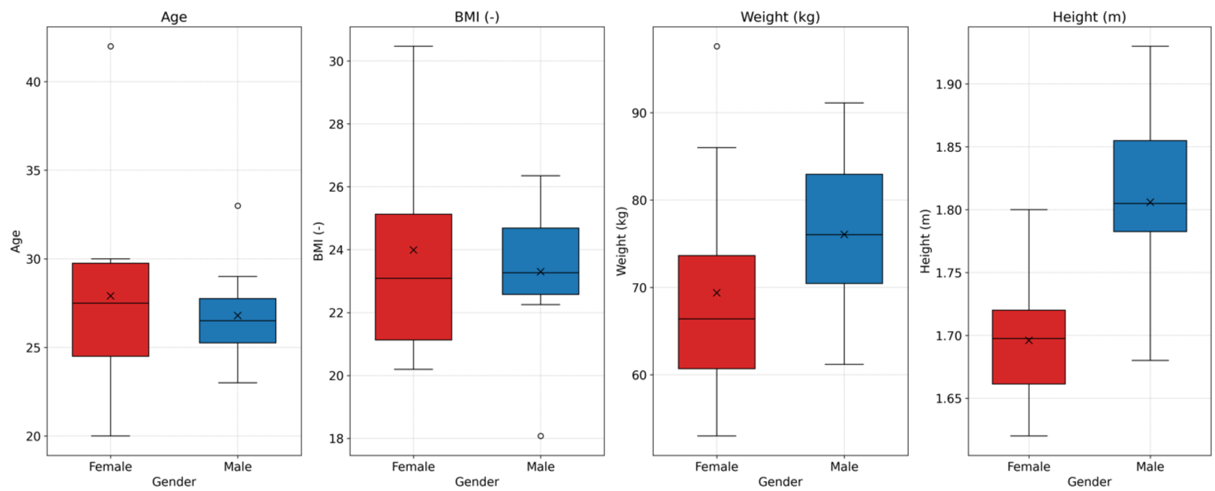

Fig. 3. Descriptive metrics of participants of volunteer study.

Each volunteer completed a total number of 14 tests. The initial two tests were designed to acclimate the volunteers to the test environment. To prevent a possible habituation of the volunteers, a different acceleration pulse (0.5 g sine pulse) was applied during this phase and a countdown prepared the volunteers for each of these two pre-tests. These familiarisation tests were conducted in the upright position, once with and once without the VR headset. After familiarisation, the main test execution began, comprising three repetitions of each combination of seat position and AEB pulse. The entire test matrix can be seen in Fig. 4b.

Compliance with ethical standards for volunteer testing was assured via the approval of the ethics committee of the Medical University of Graz, Austria (No. EK 36-095 ex 23/24).

D. Data Acquisition

Volunteer kinematics was recorded using a Qualisys 3D motion-capture system with 10 infrared cameras (Miqus M3 and M5) at a frame rate of up to 650 fps. While the manufacturer reports a 3D resolution of 0.07 mm under optimal conditions, the calibration of our system achieved average camera residuals ranging from 0.31 mm to 0.49 mm, indicating a 3D accuracy below 0.5 mm. This accuracy is considered fully adequate for the experimental requirements of this study. Each volunteer was equipped with reflecting markers, which were placed on anatomic landmarks following the guidelines given by [55]. The complete list of markers is included in the Appendix, Table AII.

In addition to kinematic data, muscle activation was recorded during the simulated AEB pulses using a wireless 32-channel surface EMG System (two Cometa Wave Plus Hubs featuring a sampling frequency of 2 kHz with MiniWave EMG and Pico EMG Sensors and Kendall H124SG single-use electrodes). Prior to sensor application, the skin was shaved and cleaned with alcohol. Sensors were applied, focusing on the muscle groups that are mainly involved in the expected forward movement of the upper torso, as well as neck rotation and bracing of the lower extremities for the tests in upright position. In the back lumbar region, sensors with longer cables were used to prevent discomfort from sensor-housing imprints on the volunteer's back. Fig. 4a show a selection of sensor placements, and a complete list of sensors used and their respective locations is provided in the Appendix, Table AIII.

Finally, the feet support forces were recorded individually for the left and right foot, using a Kistler 9306A31 force transducer (combined with a Kistler Type 5073 Charge Amplifier) with a measurement range of +/- 2 kN. The belt forces at the shoulder and at the lap belt (anchor side) were recorded using force sensors (MSC 511x/SB-16-Ti). All signals were captured using an on-sled data acquisition system DEWETRON DEWE2-M13s (Trion 1820 Multi-Input-Cards) at a sampling frequency of 20 kHz.

The belt routing over the shoulder was partly too low, compared to conventional car seats. Since the main purpose of the belt was to prevent the volunteers from falling off the sled while also maintaining the shoulder marker visibility, individual shoulder-belt adjustments were omitted and the resulting routing was deemed to be acceptable.

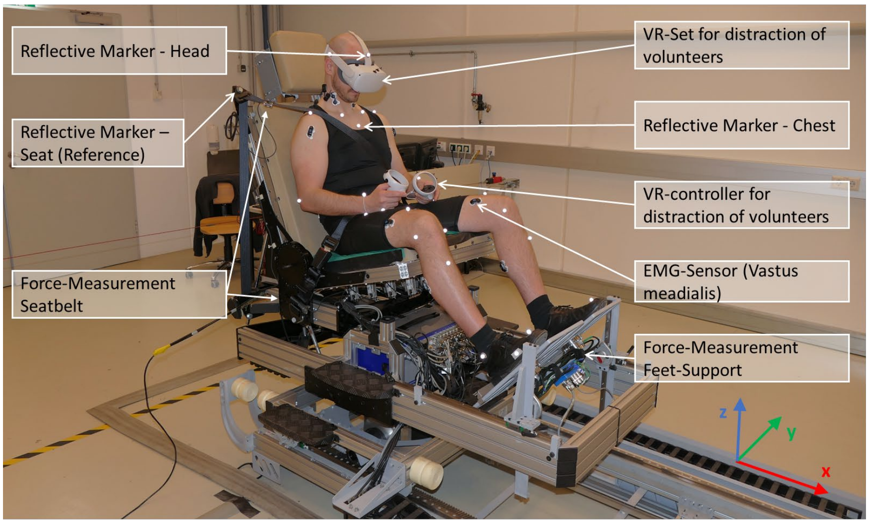

a)

	Seat position	Pulse
T0.1	Upright	0.5g sine
T0.2		
T1.1		Cluster 3
T1.2		
T1.3		
T2.1		3g/s
T2.2		
T2.3		
T3.1	Zero-G	Cluster 3
T3.2		
T3.3		
T4.1		3g/s
T4.2		
T4.3		

b)

Fig. 4. a) Test set-up (upright position) with highlighted metrics to be captured, force measurement of feet support not applicable for tests in Zero-G position. b) Test matrix conducted with each volunteer.

E. Analysis Methods

Head and chest trajectories were analysed as key landmarks of forward deflection of the volunteer. The head marker was thereby attached to the volunteer's forehead at mid-saggital plane. The chest marker was placed on mid-sternum. X- and z-excursions of these markers relative to the seat were obtained for each test. The head angle, as indicator for neck bending, was calculated based on the relative motion of the lateral (on temporal bone just above the ear) markers and the frontal head marker. The hip-motion was captured using markers on each side (ASIS) and at the front, however capturing these makers over the relevant time proved to be difficult due to obstructed visibility (belt, hands, etc.). Mean curves over the three tests with the same boundary conditions (seat position and pulse (e.g. T1.1, T1.2 and T1.3)) were calculated for each volunteer, whereby experiments, in which single markers were not tracked over the relevant time range, were excluded from analysis.

The EMG signals were normalised using data of MVC (maximum voluntary contraction) measurements. Separate sequences for each muscle group (left and right) were performed, replicating the actual sitting position and body posture. The detailed description of the procedure and the respective activation thresholds are provided in the appendix in Table AIV. As result of the EMG measurements during the sled tests, the activation time and the amplitude in percentage of MVC were calculated. The activation time was defined consistent with [56], as the time at which the signal averaged over a time window of 50 ms exceeded a threshold of 2.5 times the standard deviation of the signal during the neutral phase before the AEB loading.

In addition to the analysis of the time-based force-curves of the seat belts and the feet force loadcells, descriptive metrics were derived. For the feet-force, the initial force values at the beginning of the experiments (static weight of feet + initial bracing), the peak force as well as the timing of the peak force was measured for the left and right foot, respectively. Accordingly, the peak force and time were derived for shoulder and lap belt. For the Zero-G seat position, no feet forces were measured.

The different datasets for all experiments were compiled to a large table of metrics, which built the foundation for the further analysis of the data.

All data underlying this study—including raw measurements, test videos and photos, and processed kinematic curves —are publicly available via the TU Graz repository and can be accessed through the following DOIs: doi:10.3217/1bczm-1ab332024, doi:10.3217/mtmb0-tjb872024 [57]–[58]. In addition, a finite element model (LS-Dyna) of the test setup is provided on the OpenVT platform (https://openvt.eu/fem/lowg-volunteer-sled) to enable reproduction of the experiments using HBMs and thereby helps to validate active HBMs.

III. RESULTS

The variety of tested parameters in the volunteer study (low vs. severe AEB pulse, upright vs. Zero-G seat position, and female vs. male volunteers) resulted in a broad range of different occupant responses, kinematics, muscle activation and reaction forces. After completion of all tests, no volunteers reported experiencing any discomfort. Within the test repetitions, some volunteers did show very consistent behaviour, in contrast to others, where a large test scatter was evident. In general, no signs for habituation could be identified. The presentation of the results here is subdivided respectively and starts with the upright seat position.

A. Upright seating position

(1) Kinematics

Fig. 5 shows the kinematic response obtained from the volunteers in the upright seat position for the two different AEB pulses, whereby for all diagrams the motion relative to the seat is plotted. The curves of head excursion (Fig. 5a and b) show similar shapes as the respective AEB pulses. The timing of the peak excursions coincides with the peak accelerations very closely for the Cluster 3 pulse, whereas in the tests with the 3 g/s pulse a slight delay of about 0.2 s of the maximum head excursion is observed. Differences in the peak head forward displacement between the two pulses are seen, whereby the 3 g/s pulse led to higher x-head displacements. On average, the head excursion was approx. 200 mm in longitudinal direction for the 3 g/s pulse, and less than half of that for the less severe Cluster 3 pulse.

Within the test configurations, no clear difference between male and female volunteers was observed. Very similar tendencies, as described above, can also be observed for the chest excursion (see Fig. 5c and d and Appendix Figure B1), whereby generally the range of motion is found to be considerably less and accounts for only about half of the head displacement. For the 3 g/s pulse a slightly higher chest excursion was observed for the female compared to the male volunteers. The difference in forward displacement of head and chest results from the general upper torso rotation, but in particular for the high severity 3 g/s pulse from the considerably higher neck flexion angles observed (see Appendix, Figure B4). For the analysis of the trajectories of head and chest, the data of selected, representative volunteers are shown in Figure B5 in the Appendix. It can be seen, that despite the different pulse shapes and severities, at least in the initial phase of occupant motion the trajectory is very similar. In general, the volunteers immediately move downwards due to the compression of seat foam but also their bodies, and here a clear difference is observed for male and female volunteers. Independently of the

AEB pulse, the male participants clearly dive down further, while some female participants show some rebound upwards motion during the loading. This difference is assumed to result from the weight differences between the male and female volunteers (as seen in Fig. 3) causing different interactions with the seat foam. The longitudinal displacement of the pelvis (relative x-Waist front displacement) was approx. 10 mm for Cluster 3 and around 50 mm for the 3 g/s pulse (see Appendix, Tables BI and Figure B1), and no clear difference for male and female occupants could be identified. In general, the scatter on the results for head and chest peak displacement was quite high (values of standard deviations are reported in Table BI in the Appendix), but it could be seen that for the more severe 3 g/s pulse and also for the female volunteers it was slightly reduced. A detailed visualisation of the test repeatability for all volunteers and tests is featured in the Appendix (see Figure B7).

(2) Muscle Activity

In addition to the kinematics, the muscle activation of the volunteers was also evaluated regarding activation level and timing. The respective data are shown in as Figure B8 and Figure B9 in the Appendix. The main active muscle groups were the extensors of lower spine to neck, and the latter were activated up to about 40% MVC during the relevant pulse duration. The analysed muscles of the lower extremities (Vastus, Gastrocnimucus) – supposedly activated due to supporting the body over the feet support plate – were only activated in a range of less the 10% MVC, however a higher activation was seen when the volunteers were subjected to the 3 g/s pulse. The analysis of the onset time partly showed a very big scatter for the Cluster 3 pulse. The higher severity of the 3 g/s pulse seemed to cause a more robust muscle activation. On average, the analysed muscle groups were activated about 0.1 s after pulse start for the 3 g/s pulse and about 0.2 s later for Cluster 3.

(3) Reaction Forces

The reaction forces of the occupants with the feet support (as shown in Figure B10 in the Appendix) did show that there was very little variation amongst the volunteers regarding the initial force prior to the test. A force of about 45 N +/- 9 N was measured, and the low scatter was likely due to the fact that the feet support plates were set individually to achieve a targeted tibia angle of 55°. Regarding peak forces and timing of the latter, a clear dependency of the pulse was observed. Further, it was seen that the female volunteers on average supported themselves with less force, which is likely a result of their lower mean weight. Relevant belt forces could only be seen at the tests with the high severity 3 g/s AEB pulse (see Figure B10). However, with the observed average values of about 150 N for the shoulder belt and about 60 N for the lap belt, those forces are still considered marginal. In contrast to the lap-belt peak forces, which were more or less the same for male and female volunteers, for the shoulder-belt forces a bigger scatter was seen for the male participants. This is in line with the overall torso rotation, seen at the chest excursion. Apparently, there were more male participants who could support the AEB pulse solely by muscle activation and without being restrained by the shoulder belt.

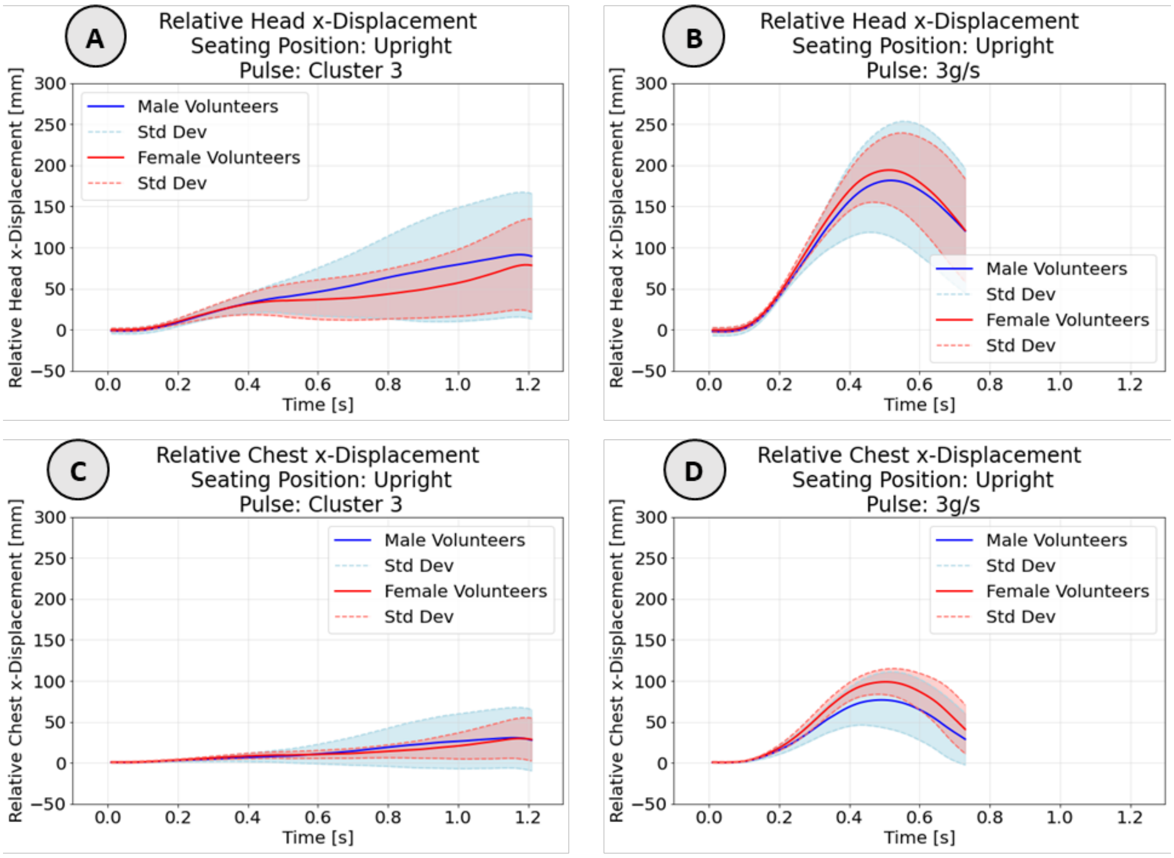

Fig. 5. Occupant responses at different braking characteristics in upright seat setting: A, B, C and D show the time-based excursions of head and chest in longitudinal direction relative to the seat motion, with its mean curves (solid lines) and the standard deviation corridor.

B. Zero-G seating position

(1) Kinematics

Fig. 6 shows the volunteer data of the experiments in the Zero-G (0g) seat setting. The focus of the analysis here is on the influence of the seat posture on the occupant response, therefore the data were analysed in comparison with the corresponding tests in the upright seat position.

Fig. 6a and b show the head excursion of the volunteers for the selected AEB pulses. As for the tests in the upright position, here also the basic shape of the curves and the timing of the peaks correspond with the pulse shape. Overall, in the Zero-G seat position lower head excursions were observed. The differences in the peak head forward displacement between the two pulses is in the same ratio, as seen with the upright seat. For the experiments in Zero-G seat setting and the 3 g/s pulse, a further head forward displacement was observed for the female volunteers. The average excursion for female participants was 100 mm, in contrast to an average of about 60 mm for the males. No such clear difference, and generally very low forward displacement, was seen for the Cluster 3 pulse.

Fig. 6c and d show the chest displacement observed in the tests in the Zero-G seat setting. It can be observed that, generally, very little chest movement of the volunteers relative to the seat is happening. With the body height axis being almost in loading direction, the torso rotation is reduced and the motion seen is predominantly a sliding down on the seatback until the pelvis is stopped. The reduced upper torso rotation induces earlier and more neck flexion (see Appendix, Figure B4) for the female volunteers, which is the main driver for the head longitudinal displacement, observed for the tests with the 3 g/s pulse. The trajectories seen in Figure B6 in the Appendix highlight the effect described above. The selected, representative male volunteer slides down the seatback with no or negligible torso rotation – the head remains in contact with the headrest at all times. In contrast, a clear neck flexion is observed in the female volunteer, resulting in further longitudinal head displacement and upwards motion relative to the seat. During that motion, the shoulder girdle is also slightly lifted, which explains the upwards z-motion seen in the chest trajectory. For the Cluster 3 pulse, as observed in the trajectory analysis of the tests in upright seat setting, the trajectories correspond to those of the higher severity pulse, but extend less. In comparison with the results in upright seat position, the scatter on the results for head and chest peak displacement is considerably less, as can be seen in Tables BI and Figure B17 in the Appendix.

(2) Muscle Activity and Reaction Forces

The analysis of the EMG signals revealed no general trend regarding the muscle activation level for the tests in the Zero-G seat position (see Appendix, Figure B8 and Figure B9). However, the highly activated muscle groups were found to be the same for both seat settings. The analysis of the onset times did show a general increase of scatter for the tests in the Zero-G position, in particular for the low severity Cluster 3 pulse. This indicates that the activation-threshold used for the definition of the onset-time was reached late or not at all for a bigger number of muscle groups and volunteers.

For the Zero-G tests, no feet support forces could be measured and, as expected, the captured belt forces, for lap as well as shoulder belt, were considered to be negligible. For completeness, the respective data are included as Figure B10 in the Appendix.

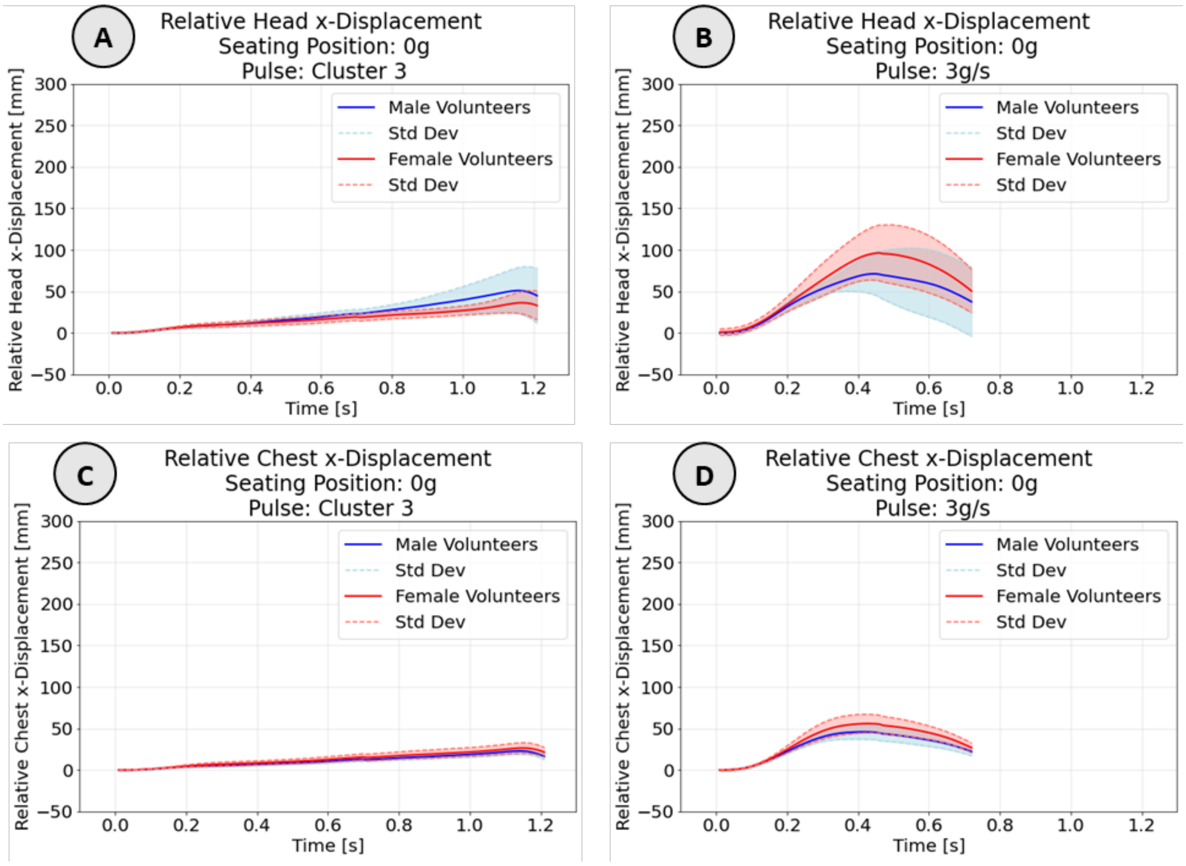

Fig. 6. Occupant responses at different braking characteristics for the zero-G seat setting: A, B, C and D show the time-based excursions of head and chest in longitudinal direction relative to the seat motion, with its mean curves (solid lines) and the standard deviation corridor.

IV. DISCUSSION

The aim of this study was to determine potential differences in the occupant response (kinematics and muscle activation) during a pre-crash braking manoeuvre in reclined and conventional upright seating postures, focusing on male and female occupants with diverse anthropometries. We approached this by conducting a total of 280 experiments, involving 10 male and 10 female volunteers in two seating configurations, and by analysing two AEB severity levels.

Limitations

This study focused on collecting kinematic, muscle and set-up-related data based on volunteer tests with the aim of providing a dataset for calibration of active HBMs, prioritising controlled laboratory conditions over in-vehicle tests. While this approach provided advantages in repeatability and measurement possibilities, tests in this environment may have some limitations. Specifically, the tests do not exactly replicate the boundary conditions and participant awareness of a real-world braking manoeuvre in a car. Participants were aware of the nature of the experiments on our inverted (sled accelerated backwards) test set-up. However, we employed a VR headset as a distraction and the participants were unaware of the acceleration onset timing, by which means we aimed to elicit a more relaxed and natural reaction.

The pure longitudinal loading is also considered to be a reasonable simplification of the process, which clearly facilitates the model calibration. However, as discussed above, it is not clear how other kinematics input (in particular, a brake-related pitching of the test vehicle) might lead to different occupant responses.

Motion capturing of the pelvis was partially obstructed by the belt and the seat, resulting in incomplete data for some volunteers, as indicated in the respective box-plot sample size in the Appendix.

Volunteer response and acceleration pulse

The head and chest excursions observed in the upright seat position were comparable with other studies [38] carried out in a laboratory environment. Further, in another recent study, carried out in a test vehicle on a track, [36], similar forward displacements of the head were reported at a braking pulse with the same onset as used in this study for the 3 g/s high severity pulse, but with considerably longer pulse duration. This supports our contention that the test duration in our experiments was long enough to capture the relevant occupant motion. For the lower severity pulse, considerably less excursion was observed, which is also in line with previous studies, such as [21] and others. The clearly bigger variation in the experiments with the lower severity pulse is an indicator that, at this low load level, the volunteers can, to some extent, maintain their posture against the pulse. While the peak values of head forward displacement are comparable for male and female volunteers, the trajectories show a clearly different curve shape, with a visible rebound effect in height axis (as seen in Appendix, Figure B5) for the females. It is assumed that this effect stems from the interplay of initial neck flexion (head CG moves downwards) and subsequent upper torso rotation (entire head is lifted until torso is fully upright). In other studies, such a difference was not reported.

Regarding the muscle activation, no pulse-dependent change in the general pattern was detected, even if slightly higher activation levels were seen for the high severity 3 g/s pulse. It was observed that the higher severity leads to a more robust activation over the entire volunteer sample – independent of gender. Considerably less variation in the timing of activation was seen for the 3 g/s pulse. The overall activation levels of the analysed muscles in the experiment, as well as the onset times, are in good correlation with this recently conducted study [36].

To derive data for the calibration of active HBMs, it is also crucial to capture further external forces acting on the volunteer, such as the feet support and the seat belt. There it was observed that relevant forces were detectable only for the higher severity 3 g/s pulse. In the experiments with Cluster 3, no relevant belt forces (<20 N) were observed for either the male or female volunteers. This was reported similarly by [38], even though their pulse was considerably more severe in comparison to our low severity pulse. Similar forces for belt as well as feet support were also reported in [29]. In our experiments, we could observe some minor gender-related differences. The feet support forces were on average higher for the males, but the shoulder-belt peak forces were slightly higher for the female volunteers. The latter is in line with the observed higher chest excursion of this occupant group.

Upright and Zero-G seating

In our experiments, a general reduction of occupant motion relative to the seat was observed for the test in Zero-G seat position in comparison with the tests in upright seat setting. This is in line with the observations of [38], but in contrast to [34–36], which studies found an increase of upper torso rotations, and thereby resulting head and chest excursions, when comparing the occupant responses in upright and far reclined seatback angles. This raises the question regarding the comparability of the results in different test environments. In addition to other influences, such as the braking pulse or a lack of pitching on our sled, a clear difference is seen in the shoulder belt mounted on the seatback, which is in contrast to the tests in the vehicles. However, as described in the Results section, we could not detect relevant peak forces in the shoulder belt for any test in Zero-G position, which also correlates with the non-locked retractors described in [38].

As also found by [36], we did not observe a clear trend towards higher or lower muscle activation levels for the Zero-G seat setting, in comparison with the upright reference, during the actual loading phase. However, [36] reported that some muscles (e.g. SCM) were considerably higher activated after the braking. In data derived from driving tests in a car, as mentioned above, this subsequent phase can still be relevant, depending on the scope of the study. But in our test environment, due to the inversion of the motion, the time range after the actual AEB pulse is not meaningful. During that period the sled has to be decelerated to a halt, which is clearly a motion that would not happen in a real driving scenario. In our experiments we could see that the variation of the results increased in the Zero-G seating, but the distribution of activation among the main involved muscle groups did not change.

We did not identify clear gender-related differences for the different seat postures. For the head excursion, a slightly higher displacement was observed for the female volunteers, going along with a different curve shape of the head trajectory, as seen in Figure B5 in the Appendix. After initially moving downwards, approximately in the angle of the seatback, the head moves upwards again as a result of neck flexion, which results in a further head forward displacement. For the male volunteers, predominantly a sliding down along the seatback was observed, until the torso is stopped when the compression of seat foam and flesh creates sufficient reaction forces. For better understanding, a sequence of the occupant motions (see Appendix, Fig. B11) has been added for selected male and female volunteers.

Outlook

Our study focused on pure longitudinal loadings, as a reasonable simplification of real-world driving scenarios. While literature includes sled tests with pure lateral loading [10–11], oblique loading [13–14], [59], and in-vehicle lane change manoeuvres [12], [24–25], [35], [56], [60–61], these were all focused on conventional upright seating positions. Therefore, future research should consider investigating occupant responses during lateral and oblique loading scenarios in novel seating positions, such as reclined.

This study was designed to serve as basis for the further development and calibration of active HBMs. Accordingly, in all phases of the test preparation and execution we aimed for an easy replication in simulation environments. The boundary conditions were very well controlled and repeatable. In the more severe pre-crash pulse, a high repeatability of the tests was observed. The anthropometry of the volunteers was captured in detail, to enable a possible morphing of HBM in the course of the calibration. The postures of the volunteers at the start of and throughout the AEB load was captured with high accuracy and for all relevant body structures. Finally, the relevant reaction forces with the environment, such as the seat-belt force and feet support, were also captured as static values (volunteer in rest position) as well as time histories to enable a verification of the model output.

V. CONCLUSION

The overall goal of this research was to analyse the occupant kinematics during the pre-crash phase in two different seating positions and with two different pulses. Our study shows a clear effect of the braking characteristics on the occupant posture at t_0, where lower excursions and higher variation of the results was observed for the pulse with lower amplitude and jerk. Forward excursions in the upright seating posture were comparable to previous studies. Smaller longitudinal motions with no, or only very small, forward rotations of the torso were observed for the volunteers in the Zero-G seat posture.

Only small differences (<10%) were observed between male and female volunteers regarding the peak forward displacement in the upright position, but there was a more pronounced rebound in height axis for the female volunteers, which is considered to be relevant with regard to interaction with the airbags. Slightly higher head excursions (+35%) were seen for the tested female volunteers, which was attributed to a more pronounced neck flexion.

This study, along with other recent work, enhances the available data on occupant kinematics during the pre-crash phase, in particular for novel and future seat settings, as well as the validity for a broader variety of occupants in terms of gender and anthropometry.

VI. ACKNOWLEDGEMENTS

Research reported in this paper was supported by the Research Consortium for Crashworthiness in Automated Driving Systems (RCCADS). The content is solely the responsibility of the authors and does not necessarily represent the official views of RCCADS or its members.

VII. REFERENCES

[1]. Richardson R, Donlon JP, Chastain K, Shaw G, Forman J, Sochor S *et al. (*2019) Test methodology for evaluating the reclined seating environment with human surrogates*. Proceedings of International Technical Conference on the Enhanced Safety of Vehicles,* 2019, Eindhoven, Netherlands.

[2]. Mroz K, Östling M, Richardson R, Kerrigan J, Forman J, Gepner B *et al. (*2020) Effect of Seat and Seat Belt characteristics on the Lumbar Spine and Pelvis Loading of the SAFER Human Body Model in reclined Postures*. Proceedings of IRCOBI Conference,* 2020, postponed (online).

[3]. Gepner BD, Draper D, Mroz K, Richardson R, Östling M, Pipkorn B *et al. (*2019) Comparison of Human Body Models in Frontal Crashes with Reclined Seatback*. Proceedings of IRCOBI Conference,* 2019, Florence, Italy.

[4]. Yamada K, Gotoh M, Kitagawa Y, Yasuki T (2016) Simulation of Occupant Posture Change during Autonomous Emergency Braking and Occupant Kinematics in Frontal Collision. *Proceedings of IRCOBI Conference,* 2016, Malaga, Spain.

[5]. Scanlon JM, Kusano KD, Gabler HC. (2015) Analysis of Driver Evasive Maneuvering Prior to Intersection Crashes Using Event Data Recorders. Traffic Injury Prevention. Issue sup2: Peer-Reviewed Journal for the 59th Annual Scientific Conference of the Association for the Advancement of Automotive Medicine (AAAM), October 2015.

[6]. Ejima S, Ito D, Satou F, Mikami K, Ono K, Kaneoka K *et al.* (2012) Effects of pre-impact swerving/steering on physical motion of the volunteer in the low-speed side-impact sled test. Proceedings of IRCOBI Conference, 2012, Dublin, Ireland.

[7]. Ejima S, Zama Y, Ono K, Kaneoka K, Shiina I, Asada H. (2009) Prediction of Pre-impact Occupant Kinematic Behavior Based on the Muscle Activity during Frontal Collision. Proc. of 21st ESV Conference.

[8]. Schoeneburg R, Baumann K-H, Fehring M. (2011) The Efficiency of PRE-SAFE Systems in Pre-braked Frontal Collision Situations. Proceedings of the 22nd ESV Conference; Washington, D.C.,

[9]. Beeman SM, Kemper AR, Madigan ML, Franck CT, Loftus SC. (2012) Occupant kinematics in low-speed frontal sled tests: Human volunteers, Hybrid III ATD, and PMHS. Accident Analysis & Prevention, **47**: pp.128–139.

[10]. Parenteau C, Shah M, Steffan H, Hofinger M. (2002) Volunteer and Dummy Head Kinematics in Low-Speed Lateral Sled Tests. Traffic injury prevention, **3**(3): pp.233–240.

[11]. Parenteau C. (2006) Far-side occupant kinematics in low speed lateral sled. Traffic injury prevention, **7**(2): pp.164–170.

[12]. Muggenthaler H, Adamec J, Praxl N, Schönpflug M. (2005) The influence of muscle activity on occupant kinematics. IRCOBI 2005.

[13]. Chan H, Devane K, Albert D, Gayzik S, Kemper A (2021) Comparisons of Initial Joint Angles and Test Buck Reaction Forces for Relaxed and Braced 5 th Percentile Female and 50th Percentile Male Volunteers and Analogous Active Human Body Models in a Simulated Drivers Seat*. Proceedings of IRCOBI Conference,* 2021, Munich, Germany.

[14]. Chan H, Albert D, Gayzik FS, Kemper AR. (2021) Assessment of Acclimation of 5th Percentile Female and 50th Percentile Male Volunteer Kinematics in Low-Speed Frontal and Frontal-Oblique Sled Tests. SAE International Journal of Transportation Safety, **9**(1): pp.3–103.

[15]. Choi, Hyung Yun, Jin Sah, Sung, lee, Bumsoo *et al.* (2005) Experimental and Numerical Studies of Muscular Activations of Bracing Occupant. International Technical Conference on the Enhanced Safety of.

[16]. Beeman SM, Kemper AR, Madigan ML, Duma SM. (2011) Effects of bracing on human kinematics in low-speed frontal sled tests. Annals of Biomedical Engineering, **39**(12): pp.2998–3010.

[17]. Ito D, Ejima S, Kitajima S, Katoh R, Ito H, Sakane M *et al.* (2013) Occupant Kinematic Behavior and Effects of a Motorized Seatbelt on Occupant Restraint of Human Volunteers during Low Speed Frontal Impact: Mini-sled Tests with Mass Production Car Seat. Proceedings of IRCOBI Conference, 2013, Gothenburg, Sweden.

[18]. Lopez-Valdes F, Juste O, Lorente A, Piqueras A, Maza M, Muehlbauer J *et al.* (2017) Short communication: Comparison of the Kinematics and Dynamics of the THOR-50M Dummy and Elderly Volunteers in Low-Speed Frontal Decelerations. IRCOBI Conference 2017.

[19]. Erlinger N, Kofler D, Heider E, Klug C (2022) Effects of Boundary Conditions and Posture on Simulations with Human Body Models of Braking Events*. Proceedings of IRCOBI Conference,* 2022, Porto, Portugal.

[20]. Rajinovic S, Safikhani S, Schachner M, Gstrein G, Kofler D, Schneider B *et al.* (2022) Testing of human reactions during braking manoeuvres combining a physical test bed with virtual reality. Frontiers in Future Transportation, **3**.

[21]. Ejima S, Koshiro O, Holcombe S, Kaneoka K, Fukushima M. (2007) A Study on Occupant Kinematic Behaviour and Muscle Activities during Pre-Impact Braking Based on Volunteer Tests. Proceedings of IRCOBI Conference, 2007, Maastricht, The Netherlands.

[22]. Morris R, Cross G. (2005) Improved Understanding of Passenger Behaviour During Pre-Impact Events to Aid Smart Restraint Development. Proceedings of the 19th International Technical Conference on the Enhanced Safety of Vehicles (ESV), Washington DC.

[23]. Kümpfbeck M, Oertel D, Pilatur K. (1999) Occupant kinematics during emergency braking. Proceedings of IRCOBI Conference, 1999, Sitges, Spain.

[24]. Reed M, Ebert S, Park BK, Jones M. (2018) Passenger Kinematics During Crash Avoidance Maneuvers. University of Michigan Transportation Research Institute Final Report. UMTRI-2018-5.

[25]. Huber P, Kirschbichler S, Prüggler A, Steidl T. (2015) Passenger kinematics in braking, lane change and oblique driving maneuvers. Proceedings of IRCOBI Conference, 2015, Lyon, France: pp.783–802.

[26]. Huber P, Kirschbichler S, Prüggler A, Steidl T. (2014) Three-Dimensional Occupant Kinematics During Frontal, Lateral and Combined Emergency Maneuvers. Proceedings of IRCOBI Conference, 2014, Berlin, Germany.

[27]. Kirschbichler S, Huber P, Prüggler A, Steidl T, Sinz W, Mayer C *et al.* (2014) Factors Influencing Occupant Kinematics during Braking and Lane Change Maneuvers in a Passenger Vehicle. Proceedings of IRCOBI Conference, 2014, Berlin, Germany.

[28]. Östh J, Ólafsdóttir JM, Davidsson J, Brolin K. (2013) Driver Kinematic and Muscle Responses in Braking Events with Standardand Reversible Pre-tensioned Restraints: Validation Data for Human Models. Stapp Car Crash Journal, **57**: pp.1–41.

[29]. Olafsdottir J, Östh J, Davidsson J, Brolin K. (2013) Passenger Kinematics and Muscle Responses in Autonomous Braking Events with Standard and Reversible Pre-tensioned Restraints. Proceedings of IRCOBI Conference, 2013, Gothenburg, Sweden.

[30]. Reed, Matthew P., Ebert SM, Jones MLH, Park B-KD. (2019) Comparison across vehicles of passenger head kinematics in abrupt vehicle maneuvers. Traffic Injury Prevention, **20**sup2S128-S132.

[31]. Carlsson S, Davidsson J (2011) Volunteer occupant kinematics during driver initiated and autonomous braking when driving in real traffic environments*. Proceedings of IRCOBI Conference,* 2011, Krakow (Poland).

[32]. Behr M, Poumarat G, Serre T, Arnoux P-J, Thollon L, Brunet C. (2010) Posture and muscular behaviour in emergency braking: an experimental approach. Accident Analysis & Prevention, **42**(3): pp.797–801.

[33]. Li M, Yang J, Zhu H) Study on Occupant Out-of-position Displacement and Injuries Under AEB Braking. In: *14th International Conference on Measuring Technology and Mechatronics Automation (ICMTMA)*2022. pp. 837–842.

[34]. Tran TD, Holtz J, Müller G, Müller S. (2022) Validation of MADYMO human body model in braking maneuver with highly reclined seatback. International Journal of Crashworthiness, **27**(6): pp.1743–1752.

[35]. Reed MP, Ebert S, Jones M, Park BK. "2021. "Occupant Dynamics During Crash Avoidance Maneuvers, Report No. DOT HS 812 997",

[36]. Ren L, Kang Y, Tan Z, Jiang C, Hu Y. (2024) Passenger muscle responses in emergency braking events with reclined seating. Scientific Reports, **14**(1): p.38.

[37]. Kang M, Lee I, Jung J, Kim S, Cho Y, Kim H *et al.* (2021) Motion Responses by Occupants in Out-of-Seat Positions During Autonomous Emergency Braking. Annals of biomedical engineering, **49**(9): pp.2468–2480.

[38]. González-García M, Siebler L, Muehlbauer J, Schick S, Peldschus S, Weber J. (2023) Kinematic response of seated male volunteers in various reclined postures on a sled subjected to a braking pulse. Accident; analysis and prevention, **193**: p.107293.

[39]. Meijer R, Rodarius C, Adamec J, van Nunen E, van Rooij L. (2008) A first step in computer modelling of the active human response in a far-side impact. International Journal of Crashworthiness, **13**(6): pp.643–652.

[40]. Meijer R, Broos J, Elrofai H, Bruijn E de, Forbes P, Happee R. (2013) Modelling of Bracing in a Multi-Body Active Human Model. IRCOBI Conference 2013.

[41]. Bose D, Crandall JR, Untaroiu CD, Maslen EH. (2010) Influence of pre-collision occupant parameters on injury outcome in a frontal collision. Accident Analysis & Prevention, **42**(4): pp.1398–1407.

[42]. Meijer R, van Hassel E, Broos J, Elrofai H, van Rooij L, van Hooijdonk P. (2012) Development of a Multi-Body Human Model that Predicts Active and Passive Human Behaviour. IRCOBI Conference 2012.

[43]. Devane K, Chan H, Albert D, Kemper A, Gayzik FS. (2022) Implementation and calibration of active small female and average male human body models using low-speed frontal sled tests. Traffic injury prevention, **23**sup1S44-S49.

[44]. Kato D, Nakahira A, Atsumi N, Iwamoto M. (2018) Development of Human-Body Model THUMS Version 6 containing Muscle Controllers and Application to Injury Analysis in Frontal Collision after Brake Deceleration. Proceedings of IRCOBI Conference, 2018, Athens, Greece.

[45]. Kato D, Nakahira Y, Iwamoto M. (2017) A study of muscle control with two feedback controls for posture and reaction force for more accurate prediction of occupant kinematics in low-speed frontal impacts, **25th ESV**.

[46]. Iwamoto M, Nakahira A, Kimpara H, Sugiyama T. (2009) Dvelopment of a Human FE Model with 3-D Geometry of Muscles and Lateral Impact Analysis for the Arm with Muscle Activity. Digital Human Modeling for Design and Engineering Conference and Exhibition.

[47]. Iwamoto M, Nakahira Y, Kimpara H, Sugiyama T, Min K. (2012) Development of a Human Body Finite Element Model with Multiple Muscles and their Controller for Estimating Occupant Motions and Impact Responses in Frontal Crash Situation. Stapp Car Crash Journal, Vol. 56.

[48]. Iwamoto M, Nakahira Y. (2015) Development and Validation of the Total HUman Model for Safety (THUMS) Version 5 Containing Multiple 1D Muscles for Estimating Occupant Motions with Muscle Activation During Side Impacts. Stapp Car Crash Journal, Vol. 59.

[49]. Devane K, Johnson D, Gayzik FS. (2019) Validation of a simplified human body model in relaxed and braced conditions in low-speed frontal sled tests. Traffic Injury Prevention, **20**(8): pp.832–837.

[50]. Paas R, Östh J, Davidsson J (2015) Which Pragmatic Finite Element Human Body Model Scaling Technique Can Most Accurately Predict Head Impact Conditions in Pedestrian-Car Crashes? *Proceedings of IRCOBI Conference,* 2015, Lyon, France.

[51]. Östh J, Larsson E, Jakobsson L (2022) Human Body Model Muscle Activation Influence on Crash Response. *Proceedings of IRCOBI Conference,* 2022, Porto, Portugal.

[52]. Graci V, Maltenfort M, Schneider M, Griffith M, Seacrist T, Arbogast KB. (2021) Quantitative characterization of AEB pulses across the modern fleet. Traffic injury prevention, **22**sup1S62-S67.

[53]. Mroz K, Östling M, Klug C, Höschele P, Lubbe N. (2022) Supplementing Future Occupant Safety Assessments with Severe Intersection Crashes Selected Using the SAFER Human Body Model. SAE International Journal of Transportation Safety, **10**(2).

[54]. Stanglmeier MJ, Paternoster FK, Paternoster S, Bichler RJ, Wagner P-O, Schwirtz A. (2020) Automated driving: A biomechanical approach for sleeping positions. Applied ergonomics, **86**: p.103103.

[55]. Qualisys AB and Bassett Biomechanics. "2021. "How to apply the Qualisys animation marker set",

[56]. Ghaffari G, Brolin K, Pipkorn B, Jakobsson L, Davidsson J. (2019) Passenger muscle responses in lane change and lane change with braking maneuvers using two belt configurations: Standard and reversible pre-pretensioner. Traffic Injury Prevention, **20**sup1S43-S51.

[57]. Gstrein G, Leo C, Kofler D, Klug C. "Dataset of Volunteer Tests - RCCADS-SINFONIA 2024, female volunteers". doi:10.3217/1bczm-1ab332024.

[58]. Gstrein G, Leo C, Kofler D, Klug C. "Dataset of Volunteer Tests - RCCADS-SINFONIA 2024, male volunteers". doi:10.3217/mtmb0-tjb872024.

[59]. Arbogast KB, Mathews EA, Seacrist T, Maltese MR, Hammond R, Balasubramanian S *et al. (*2012) The Effect of Pretensioning and Age on Torso Rollout in Restrained Human Volunteers in Far-Side Lateral and Oblique Loading. *Proceedings of 56th Stapp Car Crash Conference,* 2012.

[60]. Kirschbichler S, Sinz W, Prüggler A, Huber P, Steiner K) Detailed Analysis of 3d Occupant Kinematics and Muscle Activity During the Pre-Crash Phase as Basis for Human Modeling Based on Sled Tests. In: *International Technical Conference on the Enhanced Safety of Vehicles*2011.

[61]. Ghaffari G, Brolin K, Brase D, Pipkorn B, Svanberg B, Jakobsson L *et al.* (2018) Passenger kinematics in Lane change and Lane change with Braking Manoeuvres using two belt configurations: standard and reversible pre-pretensioner. IRCOBI conference 2018.

[62]. Cometa srl. (2020) EMG and Motion Tools - Software Manual.

[63]. Peter Konrad. "The ABC of EMG - A Practical Introduction to Kinesiological Electromyography", https://velamed.com/wp-content/uploads/ABC-of-EMG.pdf [Accessed 20 November 2023].

APPENDIX A – VOLUNTEER PREPARATION

In Table AI the anatomical measurements of each volunteer, conducted before the test, are shown.

TABLE AI
ANATOMICAL MEASUREMENTS OF THE VOLUNTEERS

Volunteer -ID	*Age*	*Weight (kg)*	*Height (m)*	*BMI (-)*	*Chest Circumference (mm)*	*Waist Circumference (mm)*	*Hip Circumference (mm)*	*Arm Length (mm)*	*Inseam (mm)*	*Knee Height (mm)*	*Pelvic Height (mm)*	*Shoulder Height (mm)*	*Foot Length (mm)*
P125M	29	72.1	1.8	22.25	918	835	850	710	890	550	970	1490	280
P130M	27	65.2	1.7	22.56	850	760	810	660	760	520	1000	1330	250
P204M	28	69.9	1.68	24.77	980	830	870	650	840	500	970	1370	245
P242M	27	83.5	1.78	26.35	955	885	950	720	980	590	1080	1510	260
P328M	25	91.1	1.93	24.46	970	880	980	730	990	580	1190	1620	270
P350M	26	79.1	1.87	22.62	900	805	915	750	900	550	1060	1480	260
P381M	24	82.2	1.86	23.76	955	880	950	770	1000	580	1110	1560	310
P854M	26	72.95	1.79	22.77	870	815	830	670	900	480	980	1440	255
P858M	23	61.2	1.84	18.08	855	765	850	710	920	550	1110	1550	265
P859M	33	83.2	1.81	25.40	995	880	960	700	860	530	1060	1500	275
P132W	28	97.6	1.8	30.12	1000	870	1110	760	890	540	1100	1515	260
P189W	29	69	1.66	25.04	980	805	910	670	745	450	1050	1390	250
P214W	27	62.8	1.73	20.98	890	682	855	700	840	500	950	1400	240
P361W	26	86	1.68	30.47	1030	860	1020	680	750	490	1050	1350	250
P532W	20	72.6	1.72	24.54	940	750	920	700	830	470	1040	1410	250
P598W	42	60	1.665	21.64	850	700	810	640	740	460	1010	1400	240
P658W	30	53	1.62	20.20	845	690	800	610	865	450	980	1330	230
P704W	24	63.8	1.72	21.57	850	700	955	700	790	460	1020	1415	250
P792W	23	55	1.65	20.20	830	670	790	640	730	440	950	1350	230
P973W	30	74	1.715	25.16	950	775	975	700	820	490	1040	1450	240

Table AII shows the marker positions for the motion-capturing system. The markers were placed on anatomic landmarks following the guidelines set out in [55]. In addition to the proposed marker positions of the Qualisys Sports Marker Set, additional markers were placed mid left and right clavicle and one marker was placed in the middle, between the left and right front waist marker. The additional markers are used to better track the movement of the volunteers. As markers on the back of the volunteers, which were originally included in the used marker set, cannot be tracked by the motion-capturing systems in seated position, these markers were removed for the tests.

TABLE AII
MOTION-CAPTURING MARKER POSITION

Number	***Position***	***Number***	***Position***
1	Head Front	22	Waist Right
2	Head Left	23	Waist Front Left
3	Head Right	24	Waist Front Right
4	Chest	25	Waist Front
5	Chest Left (clavicle)	26	Thigh Front Left
6	Chest Right (clavicle)	27	Thigh Front Right
7	Shoulder Top Left	28	Knee Out Left
8	Shoulder Top Right	29	Knee Out Right
9	Arm Left	30	Knee In Left
10	Arm Right	31	Knee In Right
11	Elbow Out Right	32	Shin Front Left
12	Elbow Out Left	33	Shin Front Right
13	Elbow In Right	34	Ankle Out Left
14	Elbow In Left	35	Ankle Out Right
15	Wrist Out Right	36	Fore Foot 5 Left
16	Wrist Out Left	37	Fore Foot 5 Right
17	Wrist In Right	38	Fore Foot 2 Left
18	Wrist In Left	39	Fore Foot 2 Right
19	Hand Left	40	Heel Back Left
20	Hand Right	41	Heel Back Right
21	Waist Left		

Table AIII shows the EMG sensor positions of the 24 measured signals. For measuring the EMG signals, two Cometa Wave Plus Hubs featuring a sampling frequency of 2 kHz with MiniWave EMG and Pico EMG Sensors and Kendall H124SG single-use electrodes were used [62]. Volunteer preparation and EMG sensor placement was done in accordance with [63].

TABLE AIII
EMG CHANNEL NUMBER AND SENSOR POSITION

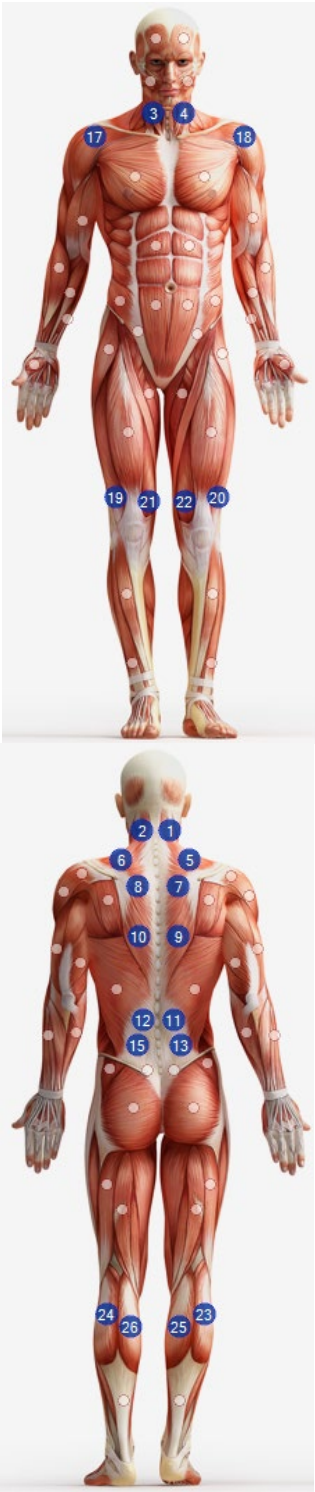

Channel	Sensor	ID	Muscle Position Left	Muscle Position Right
1	MiniWave	1		Cervical Extensor (R.Cervical Ps)
2	MiniWave	2	Cervical Extensor (L.Cervical Ps)	
3	MiniWave	3		Sternocleidomastoideus (R.Scm)
4	MiniWave	4	Sternocleidomastoideus (L.Scm)	
5	MiniWave	5		Upper Trapezius (R.Upper Trap.)
6	MiniWave	6	Upper Trapezius (L.Upper Trap.)	
7	MiniWave	7		Middle Trapezius (R.Middle Trap.)
8	MiniWave	8	Middle Trapezius (L.Middle Trap.)	
9	MiniWave	9		Lower trapezius (R.Lower Trap.)
10	MiniWave	10	Lower trapezius (L.Lower Trap.)	
11	MiniWave	11		Thoracic extensor (R.Thoracic Es)
12	MiniWave	12	Thoracic Extensor (L.Thoracic Es)	
13	MiniWave	13		Lumbar Extensor (R.Lumbar Es)
15	MiniWave	15	Lumbar Extensor (L.Lumbar Es)	
17	Pico	1		Deltoid Anterior (R.Ant.Deltoid)
18	Pico	2	Deltoid Anterior (L.Ant.Deltoid)	
19	Pico	3		Vastus Lateralis (R.Vlo)
20	Pico	4	Vastus Lateralis (L.Vlo)	
21	Pico	5		Vastus Medialis (R.Vmo)
22	Pico	6	Vastus Medialis (L.Vmo)	
23	Pico	7		Gastrocnemicus Lateralis (R.Lat. Gastro)
24	Pico	8	Gastrocnemicus Lateralis (L.Lat. Gastro)	
25	Pico	9		Gastrocnemicus Medialis (R.Med. Gastro)
26	Pico	10	Gastrocnemicus Medialis (L.Med. Gastro)	

Table AIV shows the test performed to determine the maximum activation and the respective MVC value for each muscle group for each volunteer. The volunteers were instructed to contract the respective muscle group in 3 stages of about 3 seconds duration, thereby increasing the intensity from “low” over “medium” to “full contraction”. The results of the last phase are used to normalise the EMG signals of the volunteer tests as a percentage of MVC. These tests are based on the suggestions from [63] for MVC tests, but were adjusted to our lab environment and carried out directly on the test bench. This was done to determine the MVC value in a volunteer position and posture as similar as possible to that of the volunteer tests.

TABLE AIV
MVC TEST SET-UPS TO DETERMINE THE MVC VALUE FOR EACH MUSCLE GROUP OF EACH VOLUNTEER

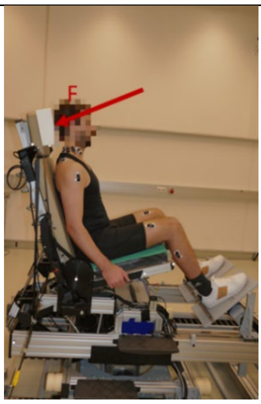	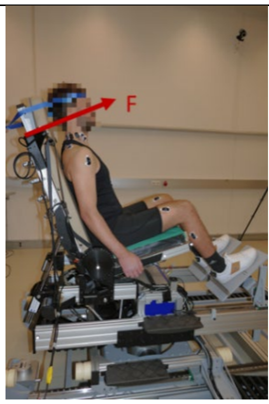	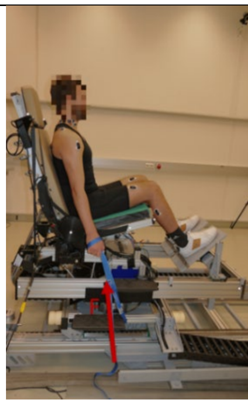
Ch2: cervical extensor, left **Ch1:** cervical extensor, right	**Ch4:** Sternocleidomastoideus, left **Ch3:** Sternocleidomastoideus, right	**Ch6:** upper trapezius, left **Ch5:** upper trapezius, right
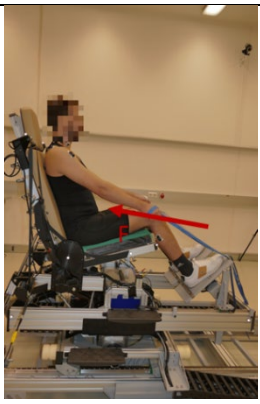		
Ch7: Middle trapezius, right **Ch8**: Middle trapezius, left	**Ch9:** Lower trapezius, right **Ch10:** Lower trapezius, left	**Ch11:** Thoracic extensor, right **Ch12:** Thoracic extensor, left **Ch13:** Lumbar extensor, left **Ch15:** Lumbar extensor, right
	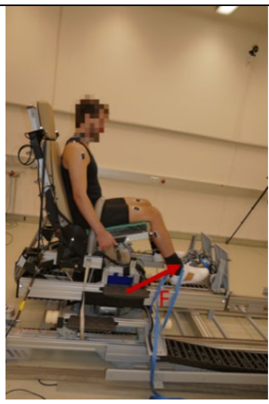	
Ch17: Deltoid anterior, right **Ch18:** Deltoid anterior, left	**Ch19:** Vastus lateralis, right **Ch21:** Vastus medialis, right **Ch20:** Vastus lateralis, left **Ch22:** Vastus medialis, left	**Ch23:** Gastrocnemicus lateralis, right **Ch25:** Gastrocnemicus medialis, right **Ch24:** Gastrocnemicus lateralis, left **Ch26:** Gastrocnemicus medialis, left

APPENDIX B – VOLUNTEER TEST RESULTS

Table BI shows the mean values, as well as the standard deviation, for head and chest marker x-displacement for the different test configurations for males and females. In addition, the time of the peak value and the time of the peak acceleration of the pulse are also given.

TABLE BI
MEAN VALUES FOR HEAD- AND CHEST-EXCURSION

		male			**female**			**time of peak_pulse**
		peak_mean	**std dev**	**time of peak**	**peak_mean**	**std dev**	**time of peak**	
		mm	**mm**	**ms**	**mm**	**mm**	**ms**	**ms**
T1	head x	91	76	1180	79	55	1190	1090
	chest x	31	37	1160	30	25	1180	1090
T2	head x	182	69	520	194	42	510	340
	chest x	77	33	490	99	16	500	340
T3	head x	51	28	1160	36	14	1170	1090
	chest x	23	4	1140	26	6	1150	1090
T4	head x	71	26	450	96	34	460	340
	chest x	456	9	410	56	11	420	340

Figure B1 shows the maximum relative x- and z-displacement for the head, chest, left and right outer knee, left and right front waist, as well as the waist front marker. The z-displacement is given at the same time as the maximum x-displacement of the corresponding marker was observed. Within the boxplots for each test configuration, all results for males and females are shown. This sums up to 30 data points for each gender and each test configuration. As some markers could not be tracked for the whole test duration by the motion-capturing systems (due to obstructions), these markers were removed from the analyses to avoid influencing the results with implausible values. For that case the number of available data points is highlighted in bold. Peak values in y-direction of motion were disregarded from analysis in this study, based on the load direction and the observed volunteer motion. The movement was tracked and is available in the public datasets [57–58].

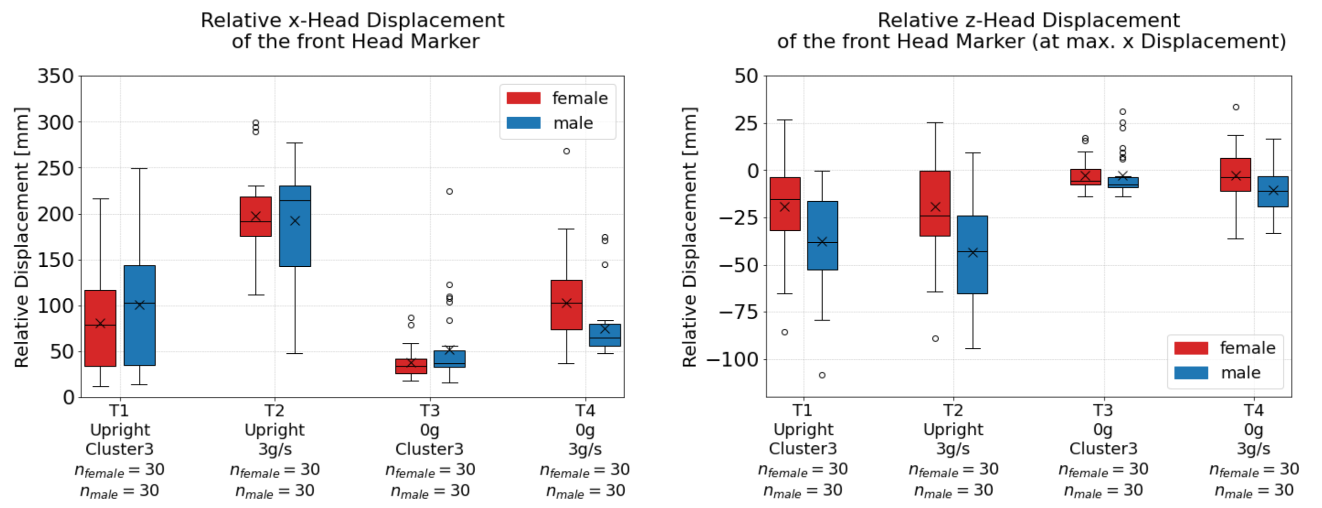

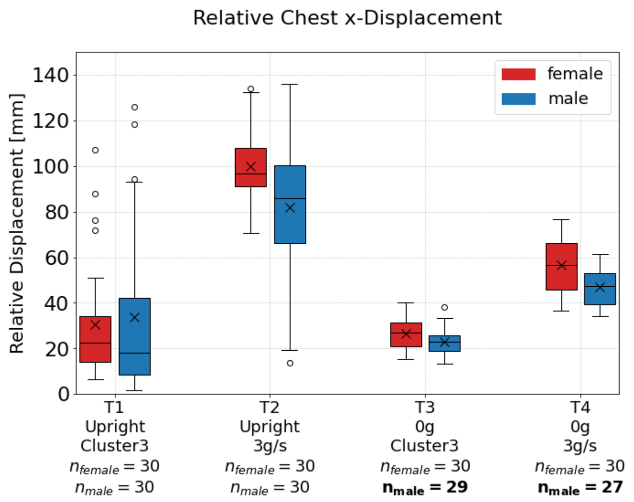
Relative Chest x-Displacement
Relative Displacement [mm]
female
male
T1 Upright Cluster3 $n_{female} = 30$ $n_{male} = 30$
T2 Upright 3g/s $n_{female} = 30$ $n_{male} = 30$
T3 0g Cluster3 $n_{female} = 30$ $\mathbf{n_{male} = 29}$
T4 0g 3g/s $n_{female} = 30$ $\mathbf{n_{male} = 27}$

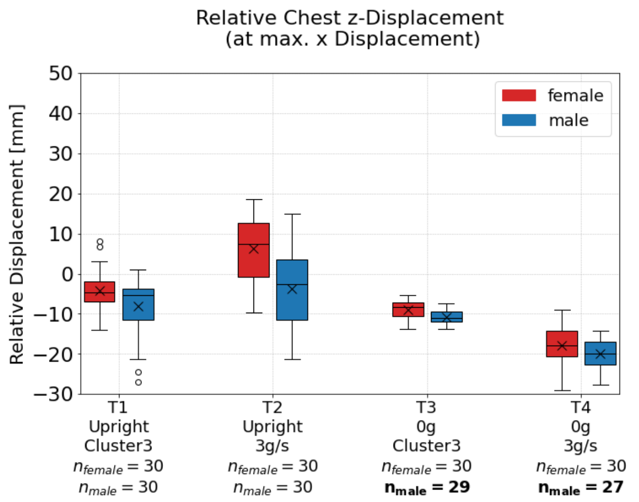
Relative Chest z-Displacement
(at max. x Displacement)
Relative Displacement [mm]
female
male
T1 Upright Cluster3 $n_{female} = 30$ $n_{male} = 30$
T2 Upright 3g/s $n_{female} = 30$ $n_{male} = 30$
T3 0g Cluster3 $n_{female} = 30$ $\mathbf{n_{male} = 29}$
T4 0g 3g/s $n_{female} = 30$ $\mathbf{n_{male} = 27}$

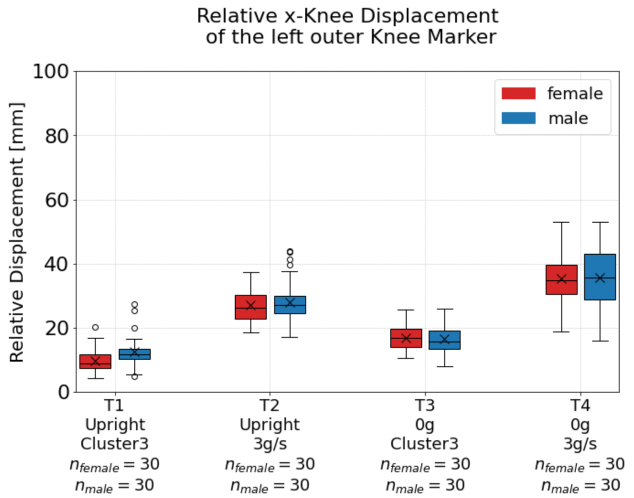
Relative x-Knee Displacement
of the left outer Knee Marker
Relative Displacement [mm]
female
male
T1 Upright Cluster3 $n_{female} = 30$ $n_{male} = 30$
T2 Upright 3g/s $n_{female} = 30$ $n_{male} = 30$
T3 0g Cluster3 $n_{female} = 30$ $n_{male} = 30$
T4 0g 3g/s $n_{female} = 30$ $n_{male} = 30$

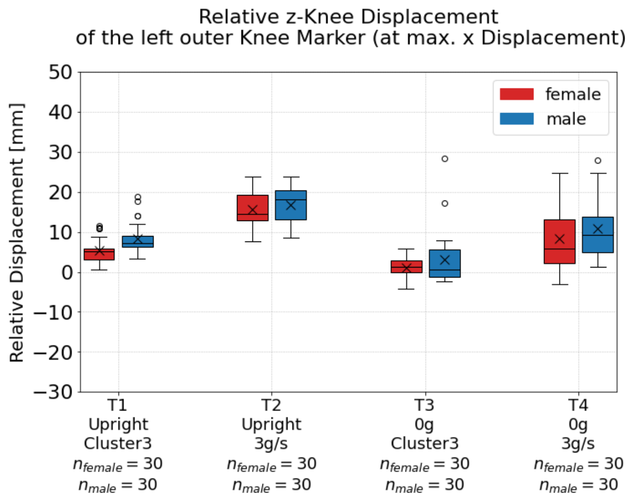
Relative z-Knee Displacement
of the left outer Knee Marker (at max. x Displacement)
Relative Displacement [mm]
female
male
T1 Upright Cluster3 $n_{female} = 30$ $n_{male} = 30$
T2 Upright 3g/s $n_{female} = 30$ $n_{male} = 30$
T3 0g Cluster3 $n_{female} = 30$ $n_{male} = 30$
T4 0g 3g/s $n_{female} = 30$ $n_{male} = 30$

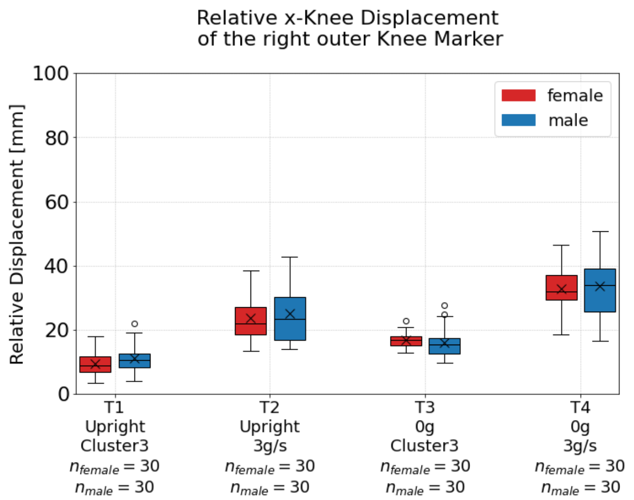
Relative x-Knee Displacement
of the right outer Knee Marker
Relative Displacement [mm]
female
male
T1 Upright Cluster3 $n_{female} = 30$ $n_{male} = 30$
T2 Upright 3g/s $n_{female} = 30$ $n_{male} = 30$
T3 0g Cluster3 $n_{female} = 30$ $n_{male} = 30$
T4 0g 3g/s $n_{female} = 30$ $n_{male} = 30$

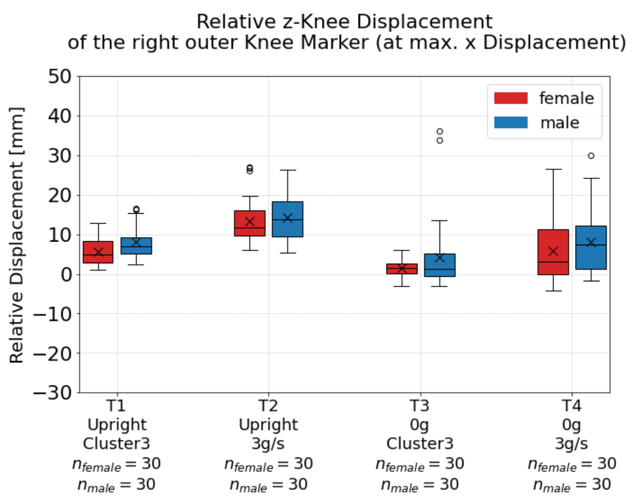
Relative z-Knee Displacement
of the right outer Knee Marker (at max. x Displacement)
Relative Displacement [mm]
female
male
T1 Upright Cluster3 $n_{female} = 30$ $n_{male} = 30$
T2 Upright 3g/s $n_{female} = 30$ $n_{male} = 30$
T3 0g Cluster3 $n_{female} = 30$ $n_{male} = 30$
T4 0g 3g/s $n_{female} = 30$ $n_{male} = 30$

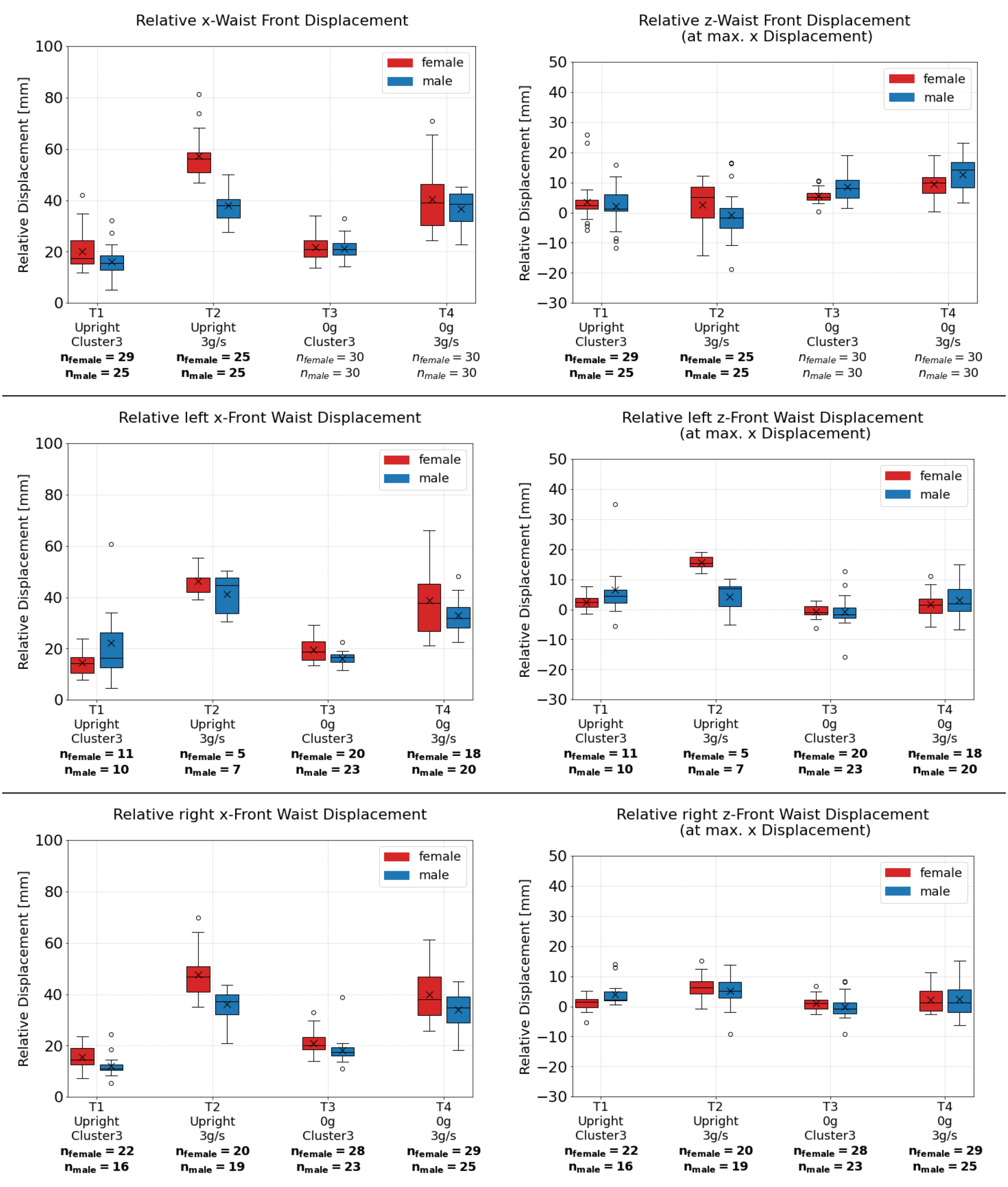

Fig. B1. Relative Displacements to Seat – Overview Peak-Values

Figure B2 shows the relative displacement in z-direction for the head and the chest marker in upright seating position with its mean curves (solid lines) and the standard deviation corridor. The curves in y-direction of motion were disregarded from analysis in this study, based on the load direction and the observed volunteer motion. The movement was tracked and is available in the public datasets [57]–[58].

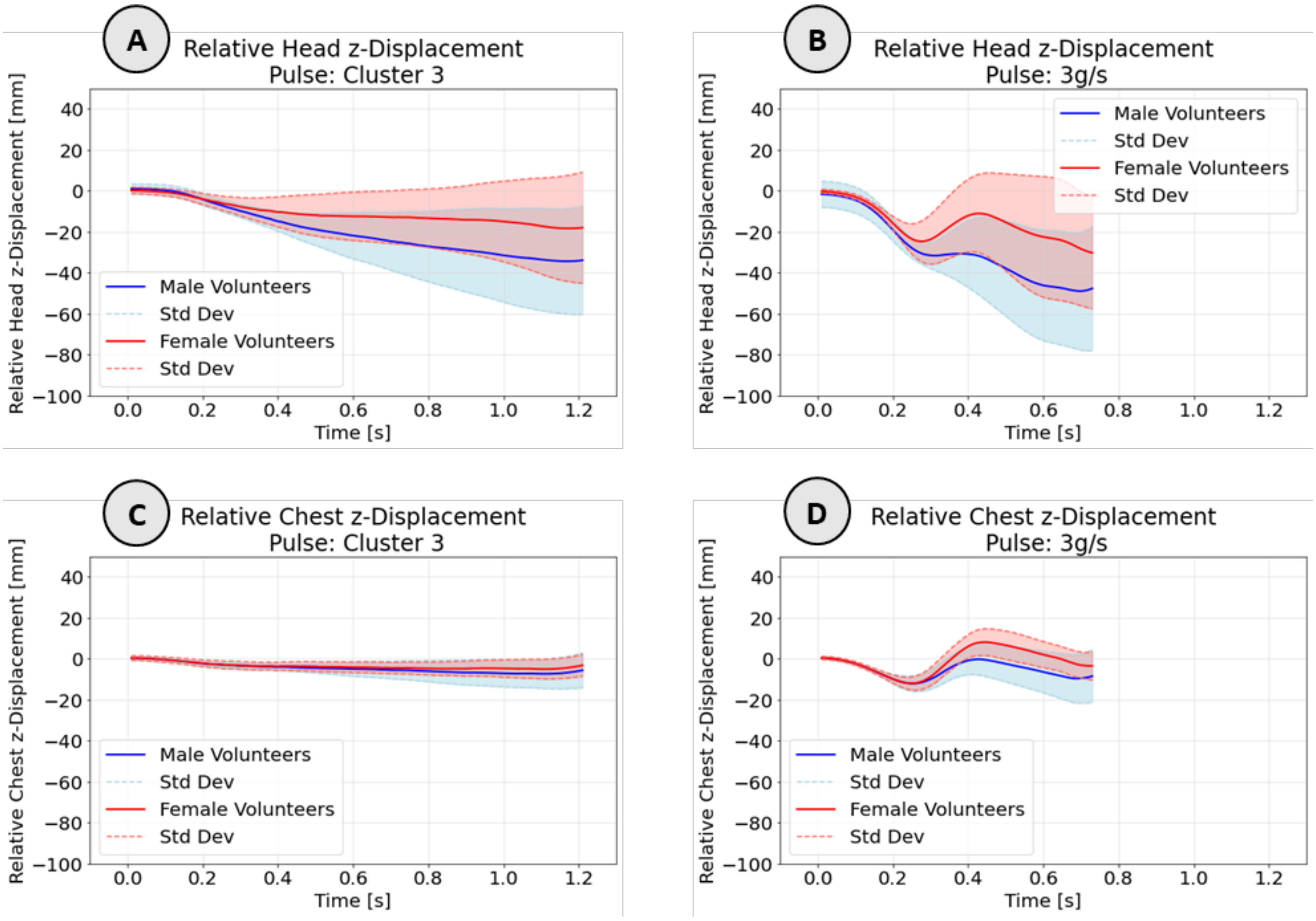

Fig. B2. Upright Seat: Relative Displacements to Seat – time-based Signals

Figure B3 shows the relative displacement in z-direction for the head and the chest marker in Zero-G seating position with its mean curves (solid lines) and the standard deviation corridor. The curves in y-direction of motion were disregarded from analysis in this study, based on the load direction and the observed volunteer motion. The movement was tracked and is available in the public datasets [57–58].

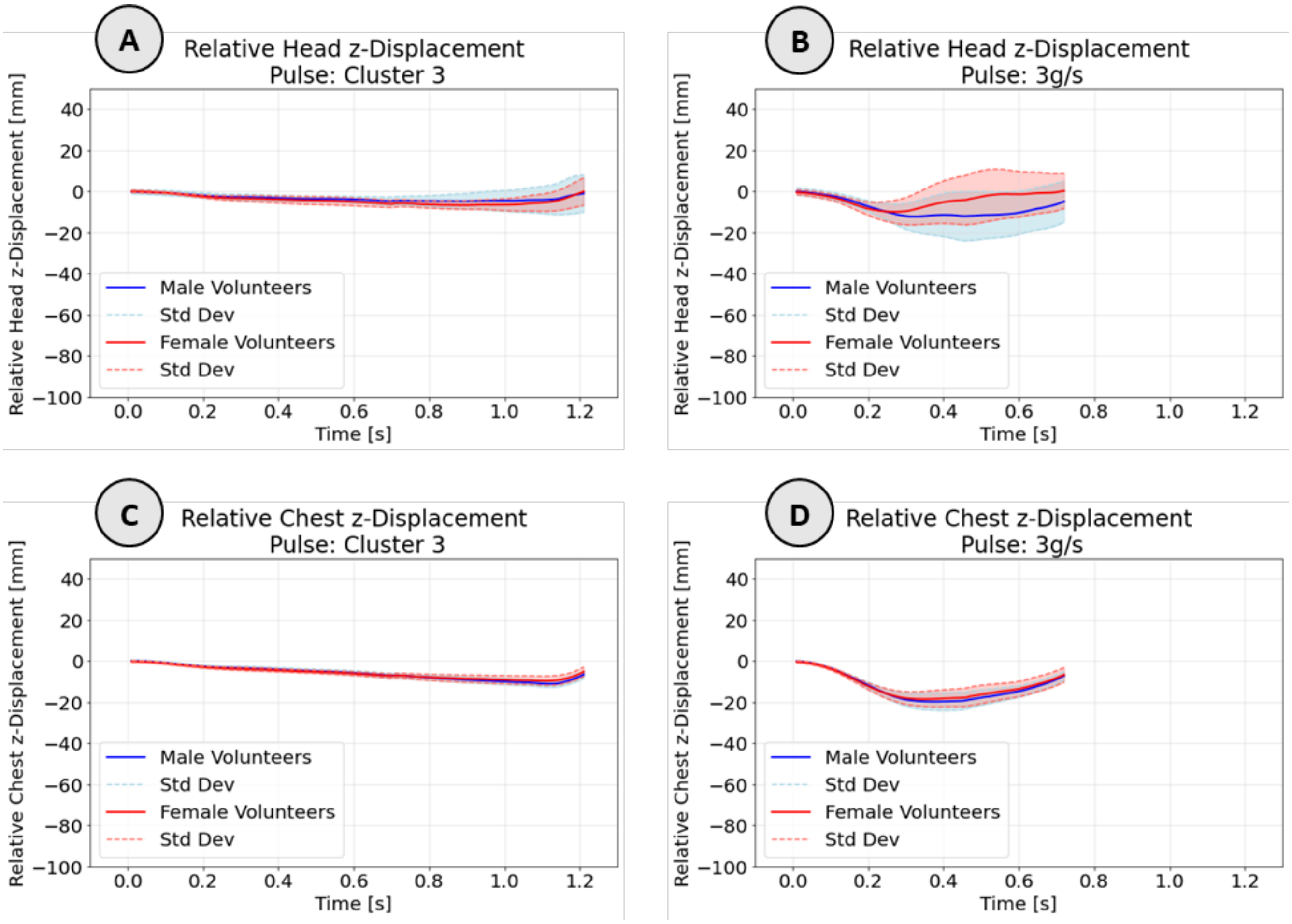

Fig. B3. Zero-G Seat: Relative Displacements to Seat – time-based Signals

Figure B4 shows the neck angle (head rotation about the y-axis, whereby positive values represent a flexion and negative values represent an extension of the neck) for all volunteers and for each test configuration. The maximum values (peak-values) as well as the time-based data are given with its mean curves (solid lines) and the standard deviation corridor. Within the boxplots for each test configuration, all results for males and females are shown. This sums up to 30 data points for each gender and each test configuration. As some markers could not be tracked for the whole test duration by the motion-capturing systems (due to obstruction), these markers were removed from the analyses to avoid influencing the results with implausible values. For that case the number of available data points is highlighted in bold.

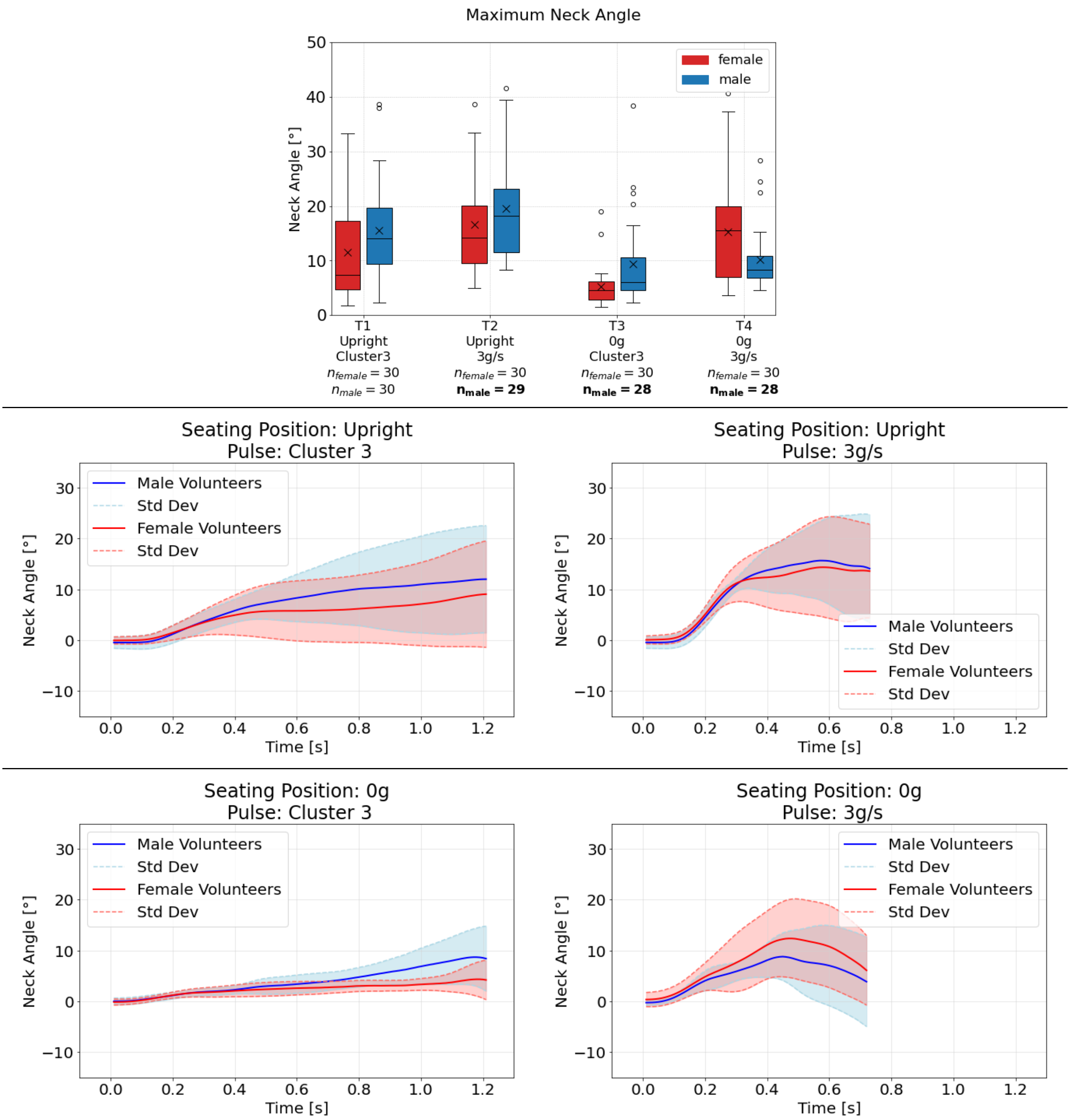

Fig. B4. Neck angle – Overview Peak-Values and time-based data

Figure B5 shows the trajectories of the front head and the chest marker for the test configurations with the upright seat. Representative male and female volunteers were selected based on the observed peak forward displacement of head and chest.

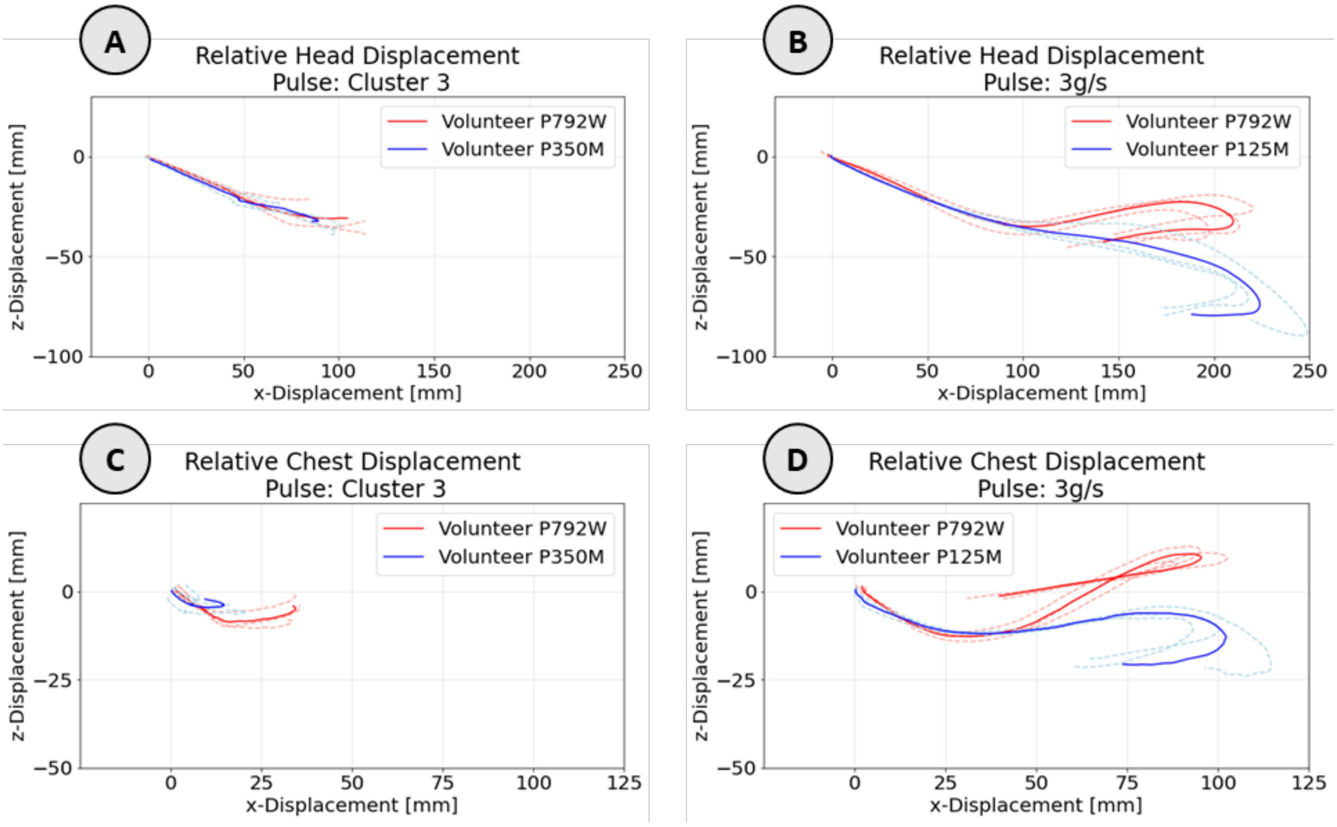

Fig. B5. Upright Seat: trajectories of head and chest for selected male and female volunteers

Figure B6 shows the trajectories of the front head and the chest marker for the test configurations with the seat in Zero-G configuration. Representative male and female volunteers were selected based on the observed peak forward displacement of head and chest.

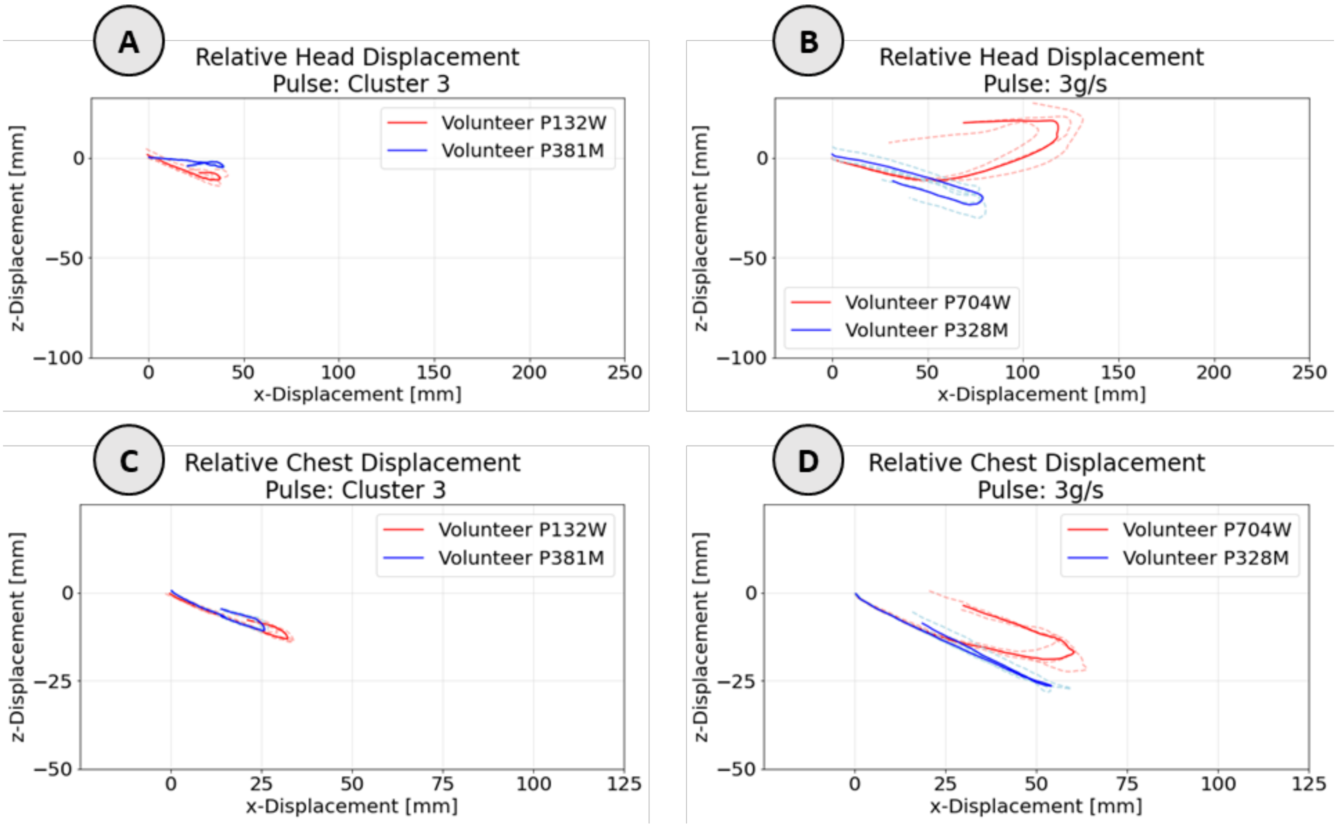

Fig. B6. Zero-G Seat: trajectories of head and chest for selected male and female volunteers

Figure B7 shows the maximum relative head and chest x-displacement for each volunteer and for each test configuration. The crosses mark the results of the three test repetitions done with each volunteer and each test configuration. This makes it possible to visualise the scatter and repeatability of the tests.

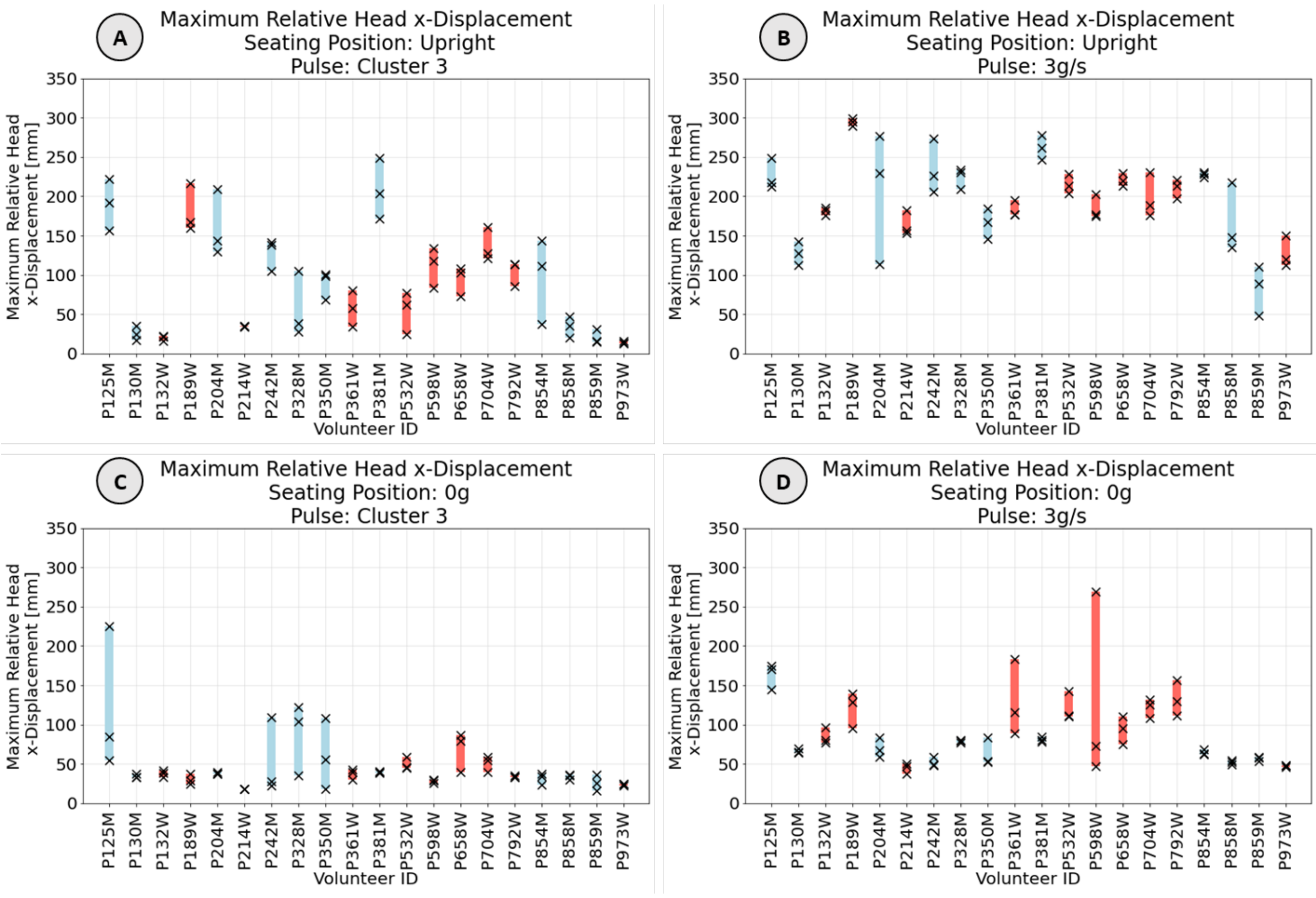

Fig. B7. Overview of variation of test results

Figure B8 shows the onset times (as defined in subclause II.E) for each muscle group, whereby data of the right and left body side are included. Within the boxplots for each test configuration, all results for males and females are shown. This sums up to 60 data points for each gender and each test configuration. The onset time was partly reached after the end of the experiment (halt of sled) or not at all. These values were removed from analysis to avoid influencing the result with implausible values. For that case the number of available data points is highlighted in bold.

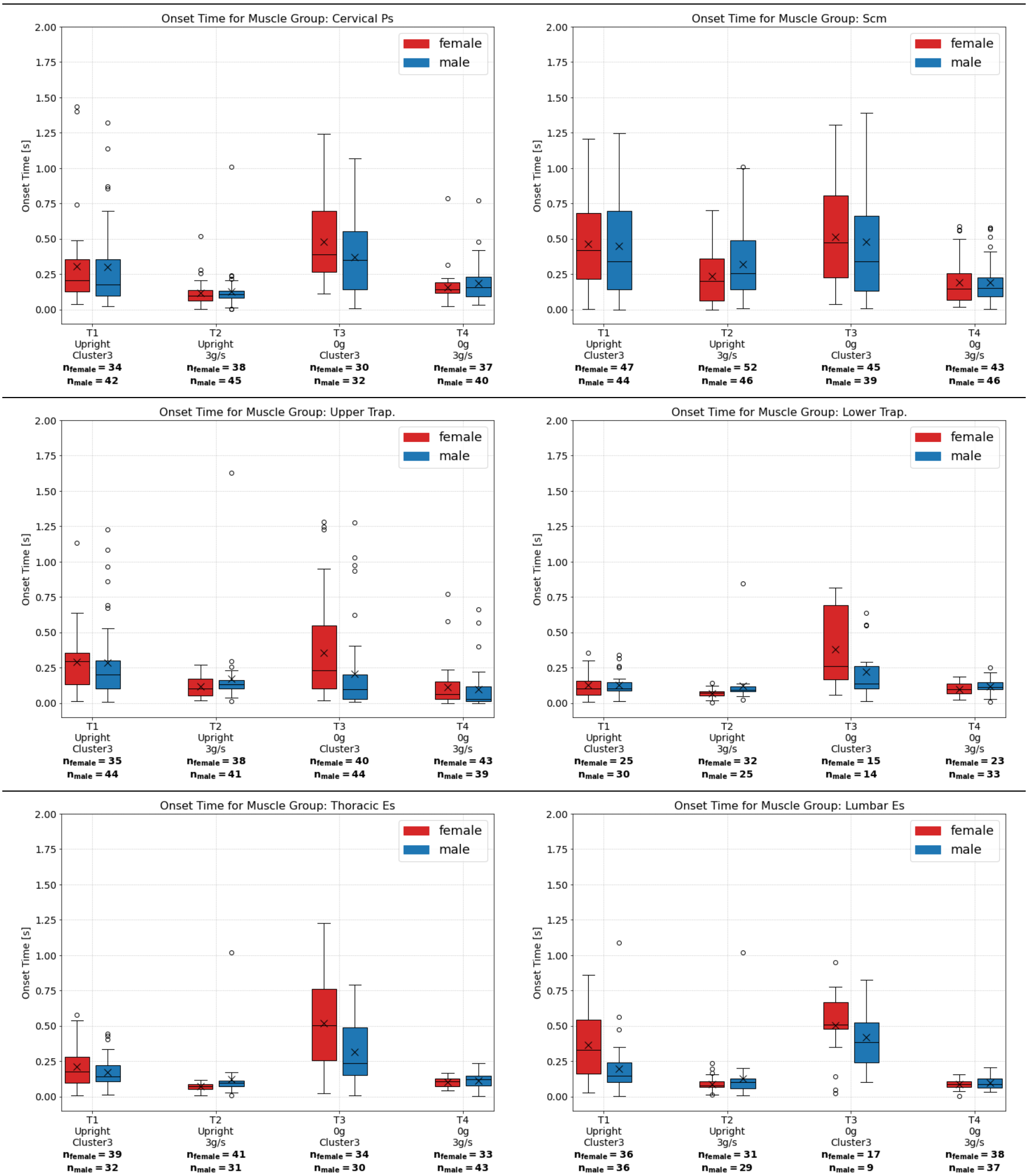

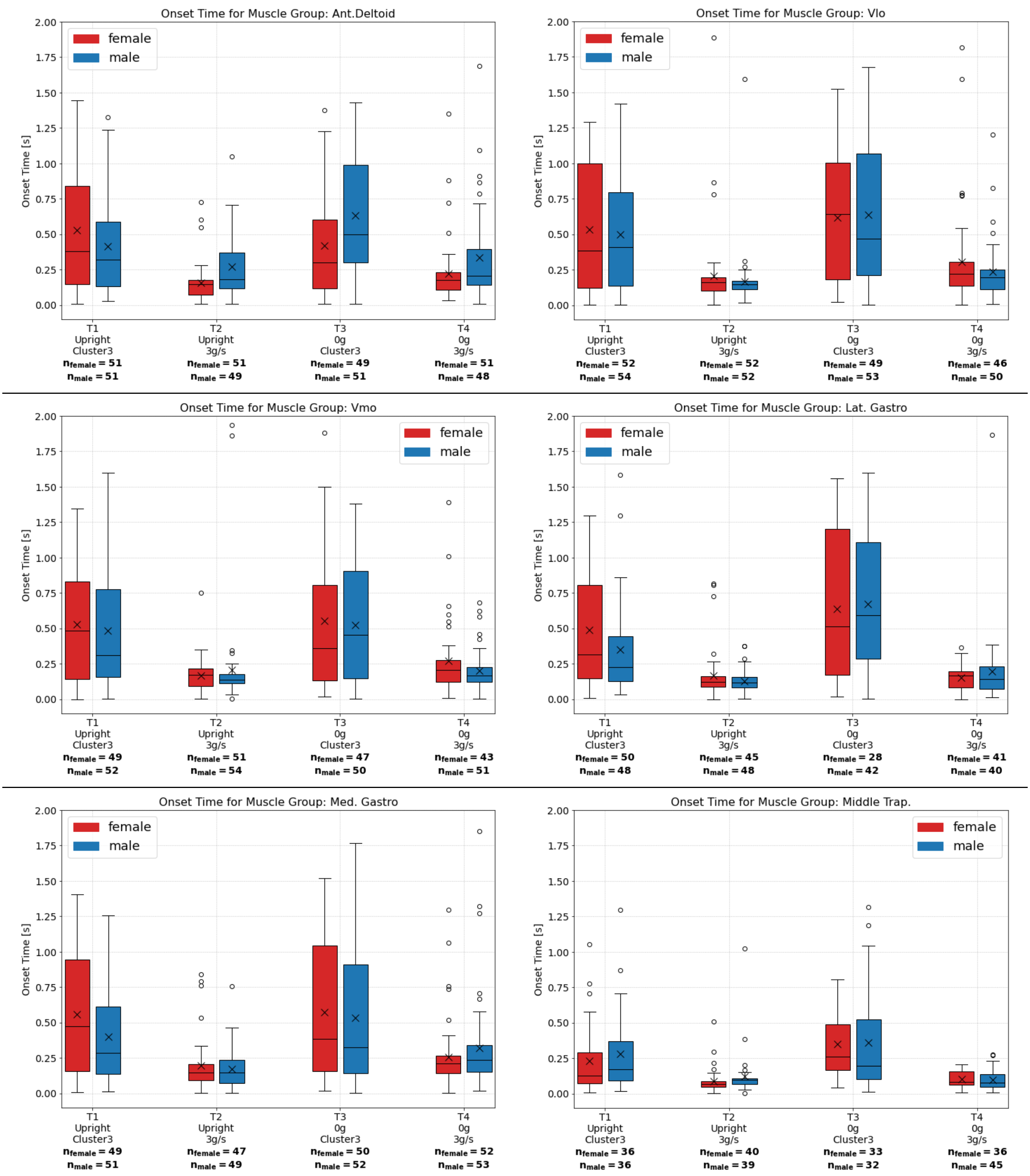

Fig. B8. Muscle Activation – Onset Times

Figure B9 shows the maximum level of muscle activation in percentage of MVC for each muscle group, whereby data of the right and left body side are included. For single experiments, an activation level higher than 100% MVC was measured, which can be explained by the MVC tests not being carried out perfectly. Those values were manually reset to 100%. Within the boxplots for each test configuration, all results for males and females are shown. This sums up to 60 data points for each gender and for each test configuration. Signals, where the onset time was not reached or was reached after test end, were excluded from analysis to avoid influencing the result with implausible values. For that case the number of available data points is highlighted in bold.

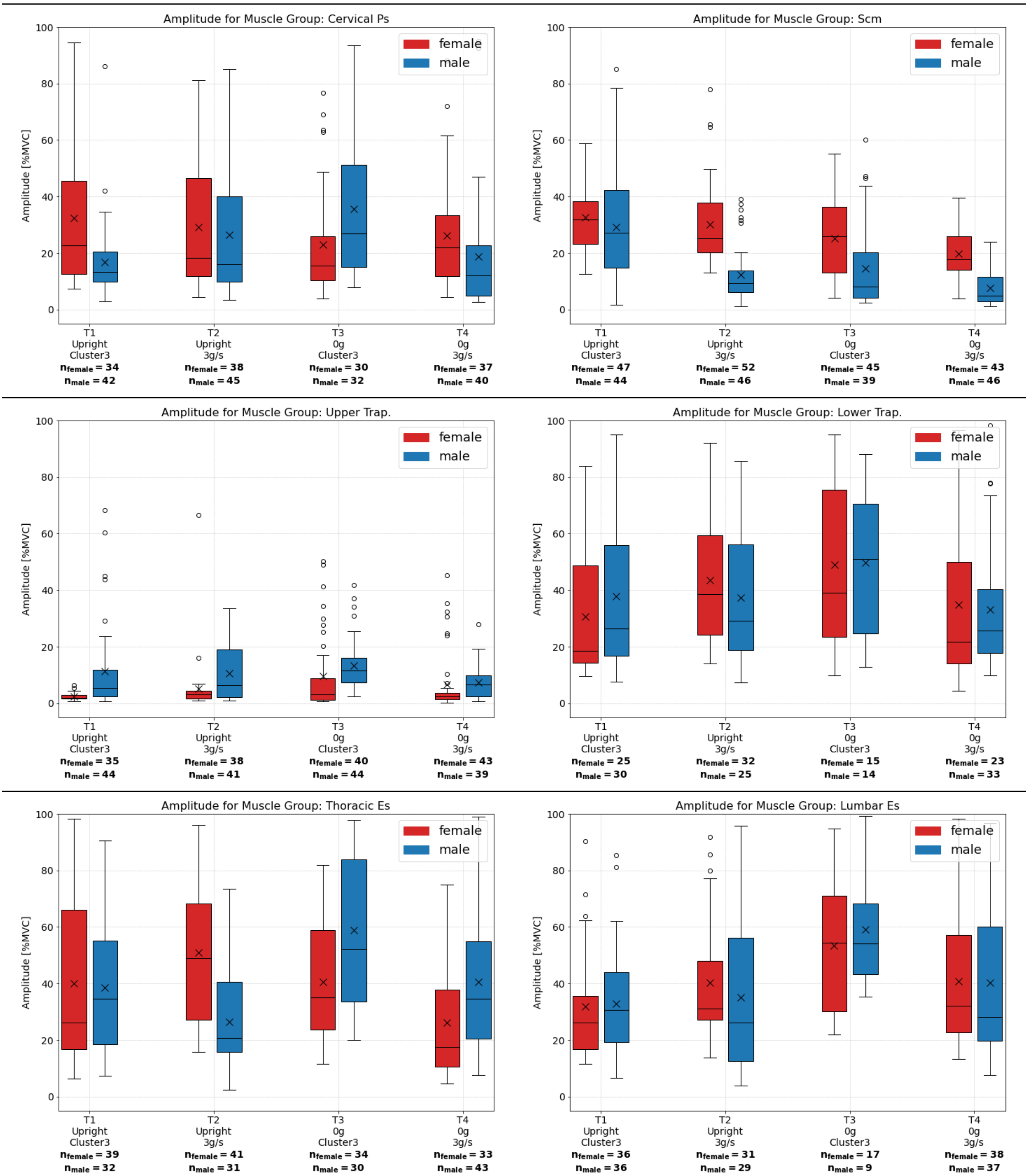

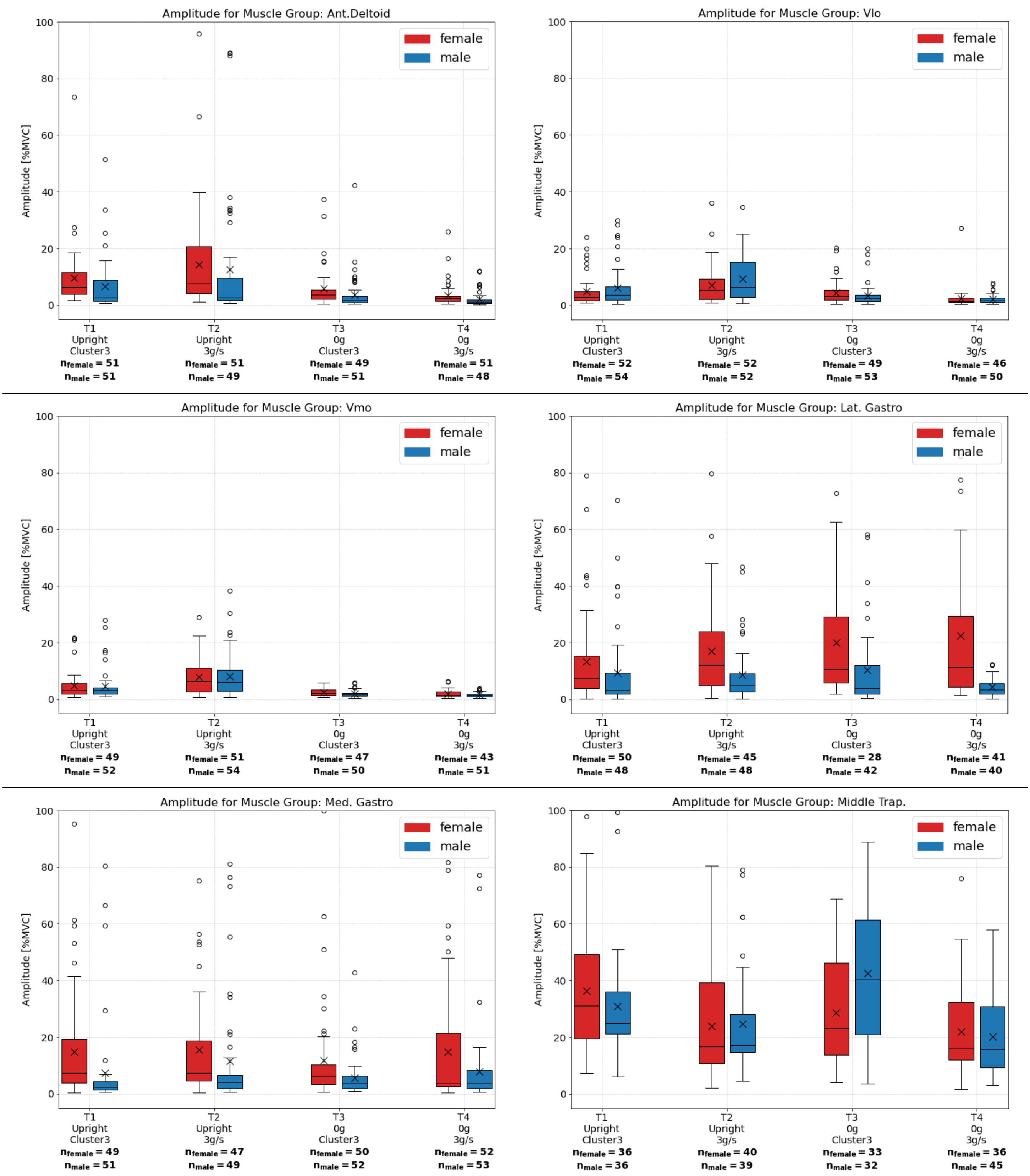

Fig. B9. Muscle Activation – Amplitude

Figure B10 shows the maximum forces detected at the shoulder and lap belt as well as the feet support. For the feet support forces, the mean value of the left and the right foot is shown, respectively. Within the boxplots for each test configuration, all results for males and females are shown. This sums up to 30 data points for each gender and for each test configuration. Respective data are available for all tests carried out, however no feet support forces were captured in the tests in Zero-G seat configuration.

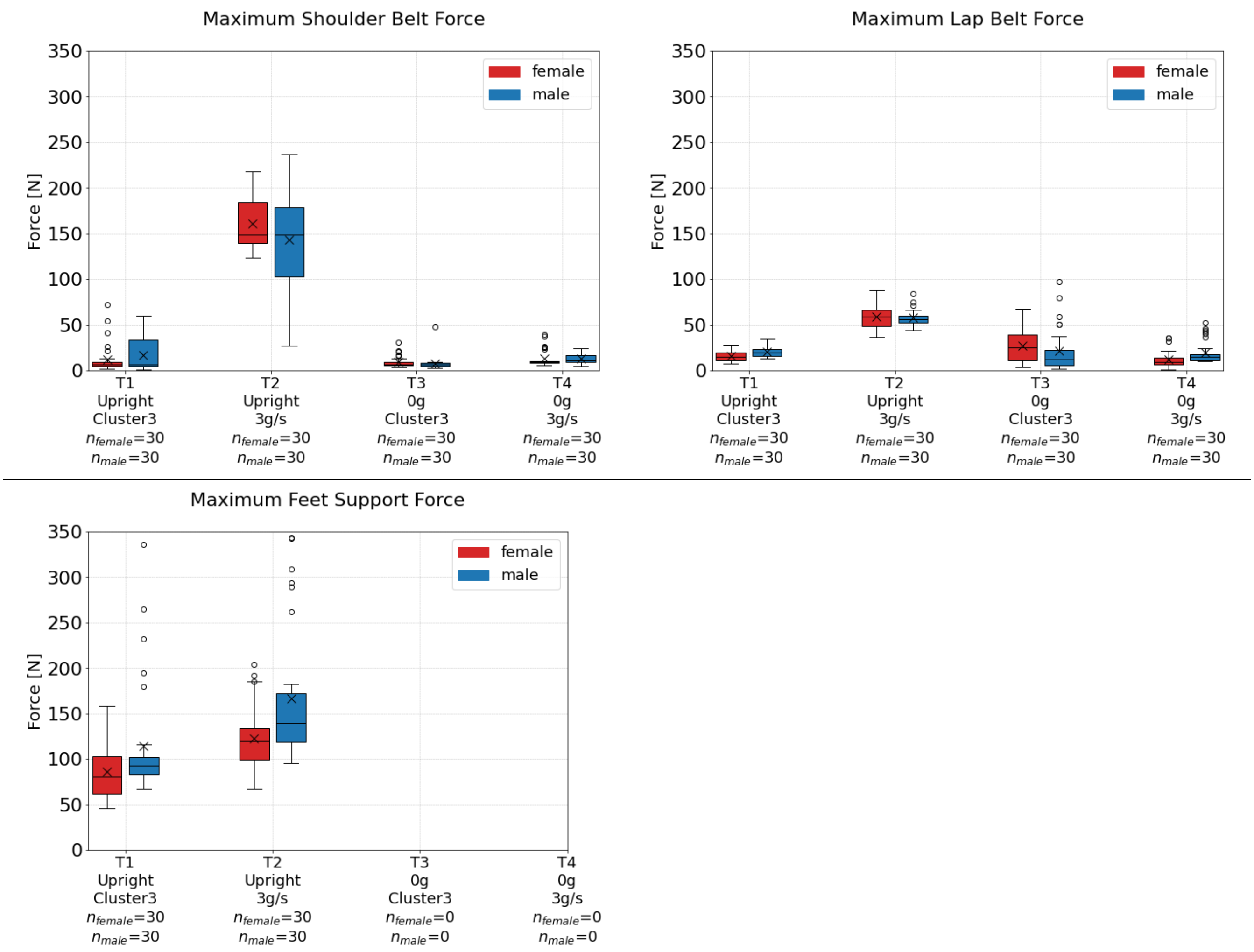

Fig. B10. Reaction forces – Peak forces

Figure B11 exemplarily shows the kinematics of selected, representative volunteers in the Zero-G seat configuration to augment understanding of the neck-angle curve data shown in Figure B4. The male and female volunteer, shown below, were selected in accordance with the data shown in Figure B6.

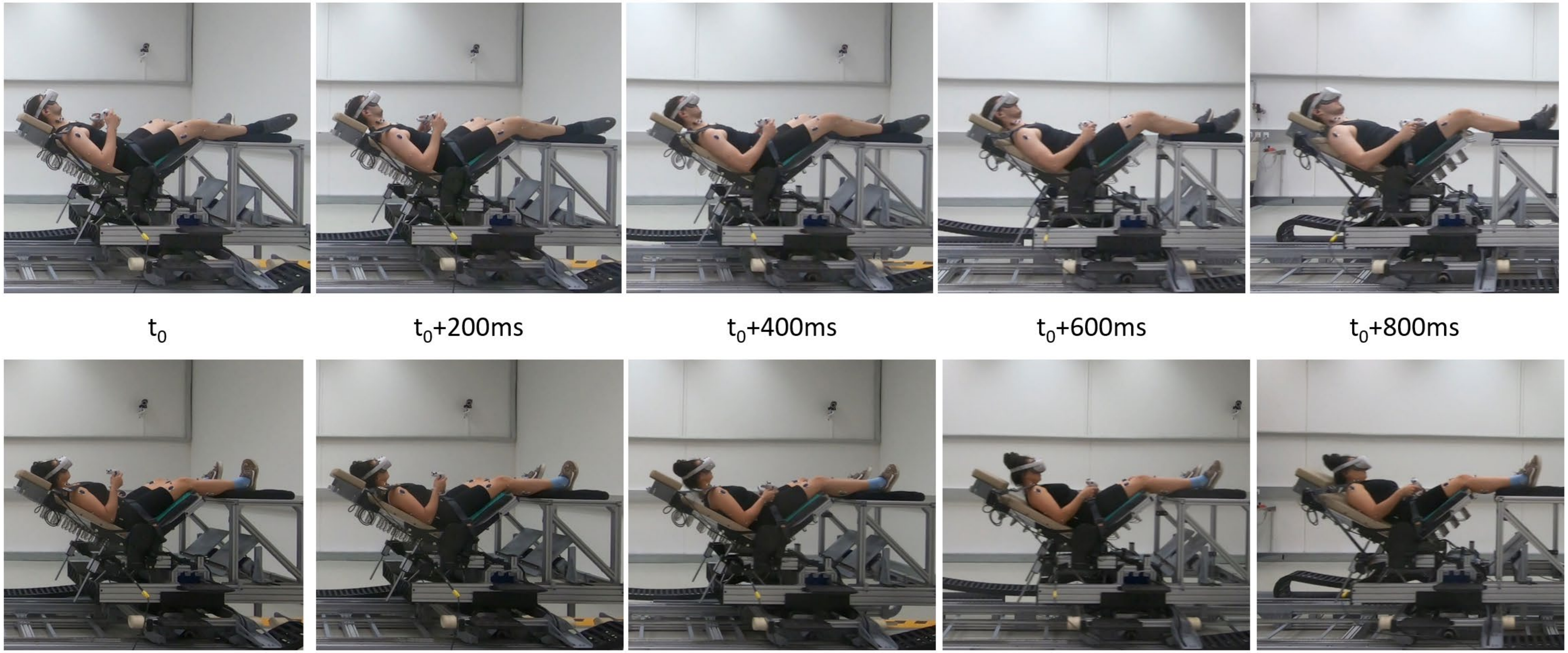

Fig. B11. Sequence of the occupant motion for selected male and female volunteers.